INSTITUTO SUPERIOR DE ENGENHARIA DE LISBOA

Área Departamental de Engenharia Eletrotécnica de Energia e Automação

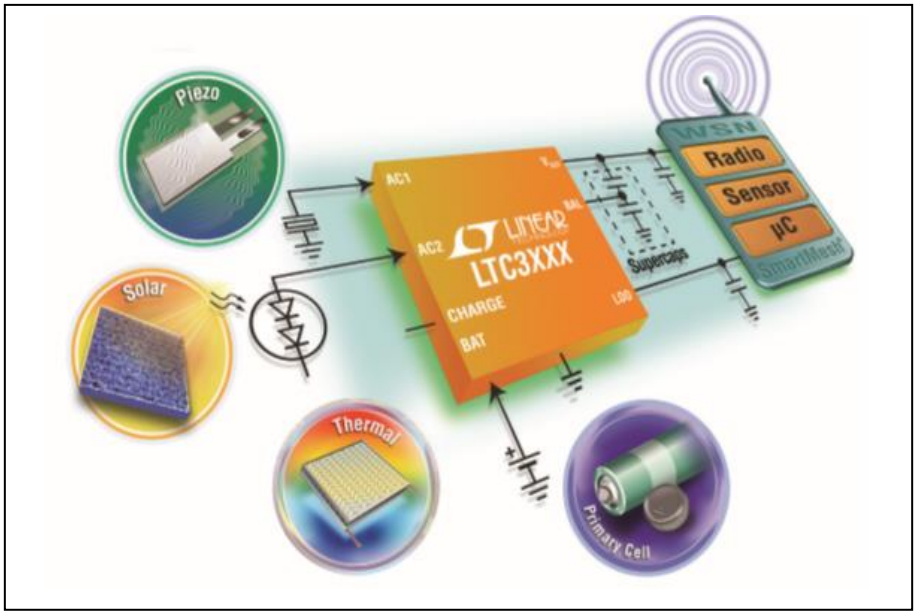

Modelling and analysis of piezoelectric energy harvester

MOHAMMAD WALEED NBOKASSEM
(Engenheiro eletrónico)

Trabalho Final de Mestrado para obtenção do grau de Mestre
em Engenharia Eletrotécnica – Energia

Orientadora:
Doutora Rita Marcos Fontes Murta Pereira
Júri:
Presidente: Doutor Luís Manuel dos Santos Redondo
Vogais:
Doutor Paulo José Duarte Landeiro Gambôa
Doutora Rita Marcos Fontes Murta Pereira

Dezembro de 2019

Resumo

Neste trabalho são apresentadas as fontes de aproveitamento de energia (*energy harvesting*) e as tecnologias existentes. É apresentado um enquadramento das tecnologias existentes no âmbito do aproveitamento de energia vibracional, nomeadamente dos sensores piezoelétricos sendo descritas as suas características. É apresentado e analisado um modelo matemático e implementado em *software* de simulação. Para validação do modelo desenvolvido é utilizado um *kit* comercial com um sensor piezoelétrico do tipo QP20W. É apresentada uma solução baseada em simulação de um aproveitamento de energia em larga escala e apontadas possíveis aplicações. É apresentada uma implementação prática de um sistema de aplicação de um sensor piezoelétrico para aproveitamento da energia gerada por vibração.

Abstract

Energy harvesting based on piezoelectric harvesters became a subject of interest in recent years, mainly due to its applications in low power devices such as wireless sensors. The harvested energy applied into piezoelectric sensors does not only depends on vibration input level but also depends on piezoelectric material properties. A description of working principle of vibration piezoelectric energy harvester is presented, starting with piezoelectric effect the discovery, type of the piezoelectric sensor and piezoelectric sensor materials. A mathematical model of piezoelectric film is addressed and implemented in simulation software in order to simulate the QP20W piezo film sensor considered in this study. The EFM32 Giant Gecko Starter Kit and Simplicity Studio® software, are used to validate the developed model and an analysis of macro-scale of piezoelectric energy harvester system is performed. A laboratorial implementation of a vibration on off switch based on piezoelectric sensor is accomplished in order to demonstrate a simple application of piezoelectric sensors.

Key-words

Energy harvesting, Piezoelectric sensors, Vibration Energy Harvesting mathematical model, EFM32 Giant Gecko Starter Kit.

CONTENTS

List of Variables

A Acceleration ($m.s^{-2}$)

A_C Contact area ($m.s^{-2}$)

A_e Electrode area (mm^2)

A_H Hamaker's constant (per unit area)

A_s Cross-sectional area of substrate layer (mm^2)

b_s Substrate width (mm)

$F_S(t)$ Vector representing existing influence of Van der Waals forces ($J.m^{-2}$)

b_p Widths of the piezoelectric layers (mm)

$\boldsymbol{C}$ Capacitance (F)

$\boldsymbol{C}$ Damping matrixes of the harvester

$\boldsymbol{C_p}$ Damping in the piezoelectric material

$\boldsymbol{C_{vdW}}$ Adhesion constant (p.u)

$\boldsymbol{D}$ Electrical displacement (C·m^{-2})

$\boldsymbol{d}$ Piezoelectric constant matrix.

$d31$ Transverse coupling mode (C. N^{-1})

$d33$ Extensional strain constant (C. N^{-1})

$\boldsymbol{E}$ Electric field (V·m^{-1})

$\boldsymbol{Ecap}$ Capacitor energy (J)

$EI(x)$ Flexural rigidity (Pa. m^3)

E_p Young's modulus of piezoelectric material (GPa)

$F(t)$ External forces vector of acting on PEH (N)

$\boldsymbol{Fe}$ Applied excitation frequency (Hz)

$H(x)$ Heaviside functions

h_s Stopgap size at the support location (μm)

I_p Electromechanical coupling term (N·C^{-1})

I_s Second moment of area (mm^4)

$i(t)$ Electric current (A)

K Harvester stiffness matrixes ($N\,.\,m^{-2}$)

L_p Piezoelectric layer length (mm)

L_s Substrate length (mm)

M Mass matrixes of the harvester (kg)

$m(x)$ Mass per unit length (kg·m^{-1})

n Constant ratio

P Polarization (C·m^{-2})

P_c Vector of nonlinear interaction in the contact pair

P_{l_s} Contact pair's nonlinear interaction force

Q Sum of external forces acting on the PEH

Q_1 Mechanical forcing (N)

R_1 Electro-mechanical coupling

R_{oc} Electro-mechanical coupling in open circuit conditions

R_{sc} Electro-mechanical coupling in closed circuit conditions

S Strain tensor

T Stress (kg·$m^{-1}s^{-2}$)

T_p Piezoelectric layer thickness (mm)

T_s Substrate thickness (mm)

t_p Thickness of piezoelectric layer (μm)

t_{pc} Distance between the neutral axis y and the piezoelectric material centre (mm)

$V(t)$ Voltage across the piezoelectric layer electrodes (V)

Wp Piezoelectric layer width (μm)

Ws Substrate width (μm)

y Distance from the neutral axis (mm)

Z Displacement vectors

α Constant ($rad.s^{-1}$)

β Constant ($rad.s^{-1}$)

ε_0 Dielectric vacuum permittivity ($F.m^{-1}$)

ξ_0 Distance between surfaces (mm)

s Elastic compliance matrix when subjected to a constant electric field ($m^2 . N^{-1}$)

ε Permittivity measured at a constant stress ($F.m^{-1}$)

$\in$ Electromechanical coupling term (N·C^{-1})

$\omega(x,t)$ Transverse deflection

$\omega_b(x,t)$ Displacement of the base

$\eta_q(t)$ Generalised modal co-ordinate

η_q Generalised modal co-ordinates

$\omega_{rel}(x,t)$ Beam displacement relative to the base

δ_{rq} Kronecker delta function

ρ_s Density of substrate material (C·m^{-3})

γ_1 Mechanical damping ratio

$\ddot{Z}$ Acceleration vectors (m.s^{-2})

$\dot{Z}$ Velocity vectors (m.s^{-1})

Chapter 1

Introduction

1 Introduction

A historic glance of piezoelectric effect

The first demonstration of the direct piezoelectric effect occurred in 1880 by the brothers Pierre Curie and Jacques Curie, shown in Fig. 1.1. They combined their knowledge of pyroelectricity with their understanding of the underlying crystal structures that gave rise to pyroelectricity to predict crystal behaviour, and demonstrated the effect using crystals of tourmaline, quartz, topaz, cane sugar, and Rochelle salt (sodium potassium tartrate tetrahydrate). Quartz and Rochelle salt were the ones that exhibited the most piezoelectricity characteristic [1].

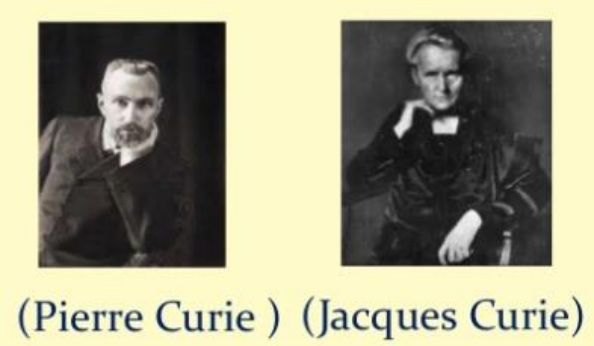

Figure 1.1- Pierre Curie and Jacques Curie [2]

The converse effect was mathematically deduced from fundamental thermodynamic principles by Gabriel Lippmann in 1881 [5]. Curies immediately noticed the existence of the converse effect [6] and went on to obtain quantitative proof of the complete reversibility of electro-elastic mechanical deformations in piezoelectric crystals.

During the next few decades, piezoelectricity remained a laboratory curiosity. More work was done to explore and define the crystal structures that exhibited piezoelectricity. In 1910 culminated with the publication of Woldemar Voigt's Lehrbuch der Kristallphysik [7], which described the 20 natural crystal classes having piezoelectric effect, and accurately defined the piezoelectric constants using tensor analysis.

Over the last decade there has been a rapid growth in research within the field of energy harvesting. There is a continuing increase of applications for wireless sensors, used for example, in structural health monitoring and condition monitoring.

The classic power sources for these sensors were batteries. However, they have a finite lifespan and therefore must be periodically replaced. In the near future, the cost of maintaining and replacing these batteries is seen to be impractical. The worst is the environmental impact caused by creating and disposing of such power sources. For these reasons there is an urgent need for an alternative, or at least a supplementary, power supply.

1.1 Objectives

The objectives of this dissertation are:

- Identify energy harvesting sources and characterize piezoelectric sensors;
- To develop a model for a unimorph energy harvester;
- To analyse some case studies where an energy harvester is connected to a capacitor as a mean of energy storage;
- To develop and validate an analytical model to predict the performance of uniform rectangular cantilever piezoelectric energy harvesters attached to an electrical load, represented by a resistor.

1.2 Motivation

The main motivation for this dissertation is the growing importance of piezoelectric energy harvesting and its applications on [8] ultrasonic imaging transducers, positioning systems, pressure and flow sensors (e.g. disposable blood pressure sensors), gas sensors energy harvester accelerometers (e.g. for airbag deployment in collisions) and in micropumps.

In addition these energy harvesters are also nowadays under study due to the improvement and minimization need to and of such devices. The use of thin material known as “piezoelectric” film is growing [8] and one of the most important project in this field is piezovolume [9]. This project focused on improving the production of this material. The research team was working to develop high-volume production tools in order to produce high-tech devices and faster, lighter and more efficient systems. The refereed project allowed

to produce a high efficient piezoelectric film 100 times thinner than a piece of notebook paper and that is considering as a basic component in a growing number of medical, communications, aerospace , ultrasound machines ,computer disc drives, automobile airbags and blood-pressure sensors [9].

1.3 Framework

This work is done in order to obtain a master degree in electrical engineering, in the field of energy harvesting, namely using piezoelectric device. The energy harvesting kit (EFM32 Giant Gecko Starter Kit) is used to validate the study and simulation described in this dissertation. The developed work is considered multidisciplinary, because knowledge in the area of physics, mathematics, and electronics is used to reach the proposed dissertation goals.

1.4 Dissertation Structure

This dissertation have 5 chapters. In chapter 1 the historical view about the piezoelectric effect discovery is addressed. The dissertation goals are defined and the benefits and importance of the piezoelectric effect are explained.

In chapter 2 is described the working principle of a piezoelectric sensor, some energy harvesting sources are addressed, and a study about piezoelectric actuators and sensors types is shown. A technological point of view is considered namely, regarding piezoelectric sensor and materials used in these devices manufacturing.

In chapter 3, several mathematical models are analysed, namely, direct and inverse effect of piezoelectricity, mechanical equations of motion and electrical equation and also the mathematical model a piezoelectric energy harvesting system connected to a storage capacitor. These models are used to emulate the piezoelectric sensor and to predict sensor' output.

In chapter 4 the MATLAB Simulink® model based on previous mention mathematical model is implemented in order to simulate the piezoelectric sensor (QP20W film sensor). Several case studies are considered and implemented in MATLAB Simulink®: model of QP20W piezo film in open circuit operation, piezoelectric energy harvesting system simulation connected

to a capacitor and macro-scaled of piezoelectric energy harvester. The validation is performed using the EFM32 Giant Gecko Starter Kit and Simplicity Studio® software. An on-off piezoelectric vibration switch is developed in laboratorial environment, as a piezoelectric vibration sensor application.

In chapter 5 is the conclusions about the developed work are addressed pointing out the results achieved for a vibration source of energy applied to a rectangular cantilever piezoelectric energy harvester. Conclusions are drawn also considering the existence of a capacitor as storage energy mean and also a conclusion about a macro-scale implementation case study is considered.

1.5 Software and development tools

In order to model and simulate the piezoelectric sensor, MatLab-Simulink® software is used, Proteus® software is used for electronic simulation and Simplicity Studio® software is used in some experiments using energy harvesting kit laboratory (EFM32 Giant Gecko Starter Kit).

CHAPTER 2

Energy harvesting methods

2 Energy harvesting sources and piezoelectric sensors

2.1 Introduction

'Energy harvester' is the term given to a device which converts forms of otherwise wasted energy, such as vibration , noises and voices, into useful energy – usually electrical energy. Devices which use ambient energy sources such as light, thermal and vibrational are widely reported in literature and are seen as possible replacements/supplements to batteries [4].
In this chapter a description of vibrational energy harvesting will be presented with particular emphasis on piezoelectric energy harvesters [8].

There are many technologies allowing energy harvesting, namely solar energy harvesting [10], thermal energy harvesting [11] and vibrational energy harvesting [12]. A solar energy harvesting device has the greatest power densities (about 15 µWmm^{-3}) but, if the same device is used on a cloudy day the power density is only 0.15 µWmm^{-3} . The performance of this device is going to reduce if is used indoors. For example, if used inside an office, the expected power density is only 0.006 µWmm^{-3}. To have an idea about the relationship between dimensions and energy production, piezoelectric harvesting device with a volume of 1000 mm^3, offers power densities of approximately 0.25 µWmm^{-3}. Figure 2.1 shows the comparison between a solar and vibrational energy harvesting with conventional batteries in terms of power density and life-time. It can be observed that for long-term applications battery power is not practical.

In the piezoelectric harvesting field ambient vibrations are the most used source of power. Vibrational energy harvesters make use of an electromechanical transducer and there are mainly three conventional types: piezoelectric, electromagnetic and electrostatic.

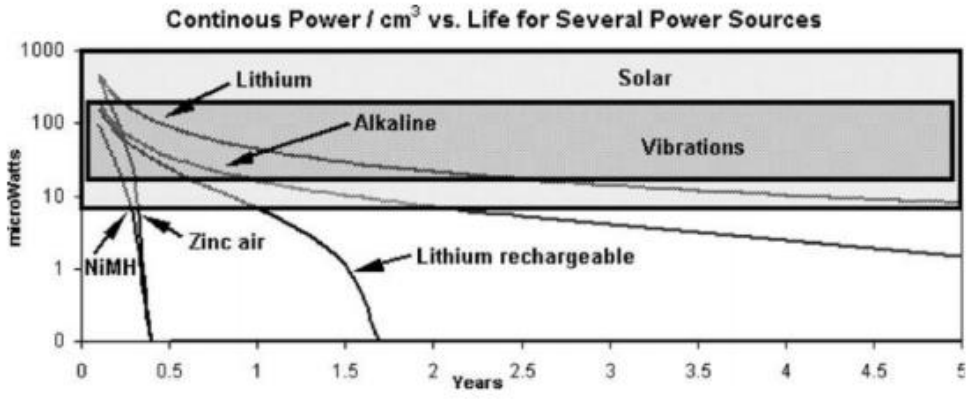

Figure 2.1- Comparison of power from solar, vibrations and various batteries [13].

2.2 Energy Harvesting Sources

A variety of energy harvesting sources are available and includes solar power, tidal waves, light energy, thermoelectricity and physical motions. Some common energy harvesting sources are depicted.

Solar Energy

Photovoltaic cells convert light energy into electrical energy and are quiet. Especially for outdoor applications, solar photovoltaic panels have been proved their merit for large scale energy harvesting. Solar energy is also used for low power devices, like watches and calculators as a secondary power source. However, solar energy harvesting technologies are affected by environmental factors such as availability and intensity of light [14].

Wind Energy

Wind energy is considered as one of the most applicable renewable energy sources. Wind turbine technology has shown dramatic progress over the last decade causing wind energy to become another favourable source for large scale energy harvesting [15,16].

Thermoelectric Energy

Thermoelectric generators convert thermal gradients directly into electrical energy over the Seebeck (thermoelectric) effect. The generated voltage and power depends on the temperature difference and the Seebeck coefficient of the thermoelectric materials [17,18]. Solid state thermoelectric generators are characterized as reliable, long life and maintenance low cost.

Vibration Energy

Mechanical vibration energy always exist in the environment, including machineries, civil structures or even human motion. Indoor machinery operating environments can provide constant mechanical vibration sources for vibration energy harvesting .The area of vibration energy harvesting include mechanics, material science, electrical and include many researches from all these three disciplines [12]. Although the energy source is vibration, these three techniques are very different from each other in terms of energy conversion methods and are described as [26]:

- Electromagnetic: A magnetic field is used in this technique to convert mechanical to electrical energy. When an oscillating mass passes through a fixed permanent magnet, a voltage is produced due to varying magnetic flux according to Faraday's law.
- Electrostatic: This harvesting type is based on a variety of capacitance. A variable capacitor which is initially charged, and separating its plates by vibration, causes capacitance changes and allow extracting the electrical energy from the system.
- Piezoelectric energy harvesting method is performed by straining a piezoelectric material. These materials produce electric charge when strained by mechanical vibrations. This type of energy harvesting is the one that considered and detailed in this work.

2.3 Types of Piezoelectric actuators and sensors

Three types of cantilever beam piezoelectric generators can be considered [3]: unimorph, bimorph series and multimorph. When the sensor has only one piezolelectrical layer attached to the substrate, the device is unimorph. On the other hand, when it has two piezoelectric layers,the device is as bimorph . Multimorph structure is considered when more than two piezoelectric layers exist.

2.3.1 Unimorph structure

The basic structure of piezoelectric bending transducer is a unimorph (sometimes also called monomorph) structure. The unimorph structure consists of one active layer, one passive, and an flexible layer bonded together. The active layer is made of lead zirconate titanate – piezoceramic material (PZT)ceramics or polyvinylidene fluoride – piezoelectric polymer (PVDF) polymers with electrodes arranged on two opposite surfaces. The PZT ceramics are usually working in transverse coupling mode and less frequently in linear mode. The passive layer, also known as elastic layer, is made of material without piezoelectric properties, such as steel, aluminium, brass, or different polymers types. The side view of unimorph transducer is shown in Figure 2.2.

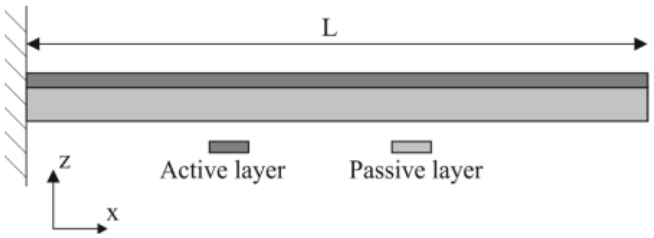

Figure 2.2- Profile of asymmetric unimorph bending transducer[19,3]

When the voltage is supplied to the electrodes of the active layer, the piezoelectric material attempts to react to the electrical signal, while being forced at the bonded surface. The net result is deflection or bending. Conversely, flexural excitation (vibrating by wrapping it) of such a device will result of electrical energy within the active layer [19].

2.3.2 Bimorph structure

The bimorph structure of piezoelectric transducer consists of two active layers, directly bonded together or separated by a passive layer. The general working principle is the same as for the previously described unimorph transducers. The side view of a bimorph transducer is shown in Figure 2.3

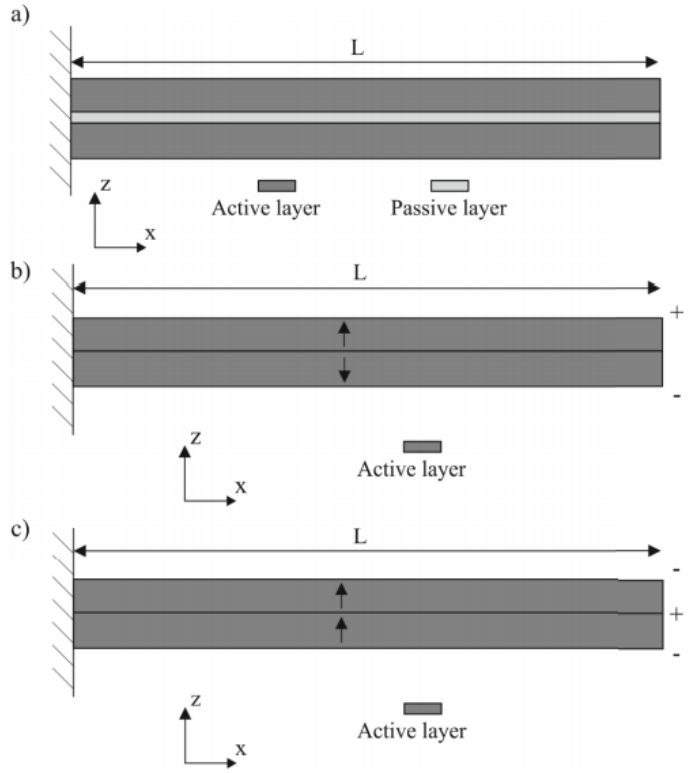

Figure 2.3 - Profile of symmetric bimorph bending transducer: a) configuration with centre passive layer, b) active layers polled and electrodes set to series operation, c) active layers polled and electrodes set to parallel operation [19,3]

When an electric field is applied to one layer of a bimorph piezoelectric it will expand, while the other layer contracts, the motional restriction along the joined surface generate forces. On the other hand, when a force is applied up on it, an electric field is generated along to the piezoelectric bimorph layer.

2.3.3 Multimorph structure

Multimorph piezoelectric transducers are based on unimorph and bimorph transducers considering multiple levels of active and passive layers, forming one structure. This type of actuator is used when large displacements and low applied voltage are needed. However, the multimorph structure offers a small resultant force and low natural frequency. When a PZT actuator is constituted by multimorph layers, it can enlarge both generated force and resonance frequency, even though, applied voltage and manufacturing cost are increased. A multimorph structure is usually bonded on top and bottom surfaces of the structures and is driven by voltages with opposite polarity. Therefore, when one is expanded, the other is contracted. Figure 2.4 shows multimorph bending transducer consisting of 52 active layers, with a symmetrical structure in the *x*-direction. The case of passive layer existing between two active layers also can be noticed in [19,3].

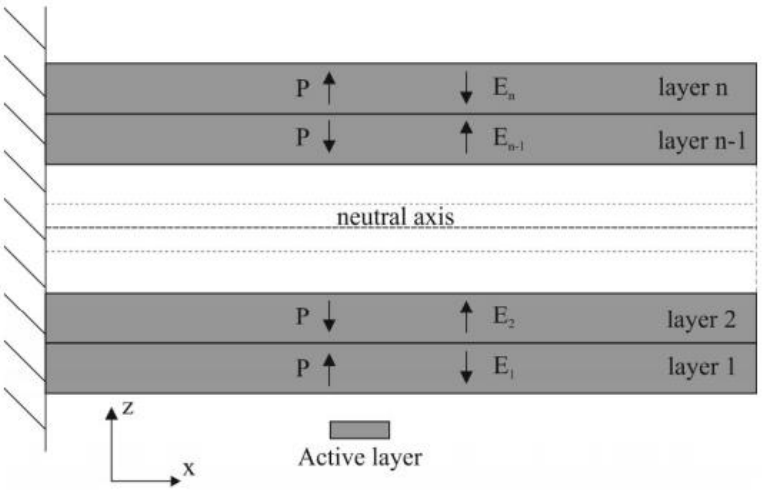

Figure 2.4 - Profile of symmetric multimorph bending transducer - [3, 19]

In Figure 2.4, the shown arrows indicate a polarization direction example and the electric field direction applied to the active layer.

2.4 Metallized Piezo Film Sheets

Piezoelectric films are available in a variety of different film sizes and thicknesses where the most common values are between 28 and 52 µm, due to their higher capacitance and good mechanical qualities. Thick film of 110 µm is used where maximum strength is needed, or if the sensor is being used in a thickness mode (d33) application. Metallization options include

as silver ink that is considered best for applications where mechanical stress is being applied [20]. Considering these characteristics, metalized piezo films, can be applied into simple transducers, or used as full size sheets for applications several applications, namely in speakers [20].

In table 2.1 is shown an example of the film dimensions according to the model and film material.

Table 2.1 – Dimension of Piezo Film Sheets [20]

	DIMENSIONS in INCHES (mm)						
Description	A Film	B Electrode	C Film	D Electrode	t (µm)	Metallization	Part Number
28 µm piezo film	8.00 (203)	8.00 (190)	11.00 (280)	11.00 (267)	28	Cu-Ni	1-1003702-7
28 µm piezo film	8.00 (203)	7.50 (190)	5.50 (140)	5.00 (127)	40	Silver Ink	1-1004347-0
28 µm piezo film	8.00 (203)	7.50 (190)	11.00 (280)	10.50 (267)	40	Silver Ink	1-1004346-0
52 µm piezo film	8.00 (203)	8.00 (190)	11.00 (280)	11.00 (267)	52	Cu-Ni	2-1003702-7
52 µm piezo film	8.00 (203)	7.50 (190)	5.50 (140)	5.00 (127)	64	Silver Ink	2-1004347-0
52 µm piezo film	8.00 (203)	7.50 (190)	11.00 (280)	10.50 (267)	64	Silver Ink	2-1004346-0
110 µm piezo film	8.00 (203)	8.00 (190)	11.00 (280)	11.00 (267)	110	Cu-Ni	3-1003702-7
110 µm piezo film	8.00 (203)	7.50 (190)	5.50 (140)	5.00 (127)	122	Silver Ink	3-1004347-0
110 µm piezo film	8.00 (203)	7.50 (190)	11.00 (280)	10.50 (267)	122	Silver Ink	3-1004346-0

2.4.1 Packaged piezoelectric actuators and sensors

Considering packaged piezoelectric actuators, the model QP20W shown in figure 2.5 is one of the most common bimorph actuator used.

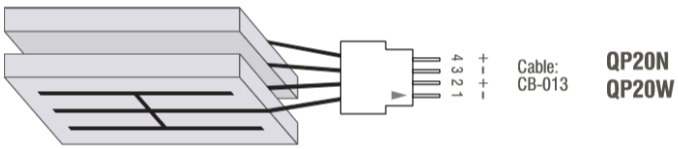

Figure 2.5 – Structure of DT series of piezo film sensors [34]

The packaging process electrically isolates the piezoelectric ceramic, and allows the device to be used in otherwise difficult environmental conditions including submerged applications [34].

2.4.2 DT Series Elements

The DT series of piezo film sensors elements are rectangular elements of piezo film with silver ink screen printed electrodes. They are available in a variety of sizes and thicknesses and a representation of this referred structure is shown in figure 2.6.

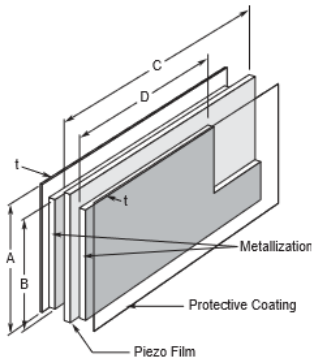

Figure 2.6 – Structure of DT series of piezo film sensors

2.4.3 DT Series Elements with Lead Attachment

DT series of piezo film sensors elements with lead attachment are basically the same as the DT series elements, having silver ink screen printed electrodes, and they are also available in a variety of different sizes and thicknesses. Lead attachment is accomplished using a riveted handle going 300 mm of 28 American wire gauge (AWG) wire and a representation of this referred structure is shown in Figure 2.7.

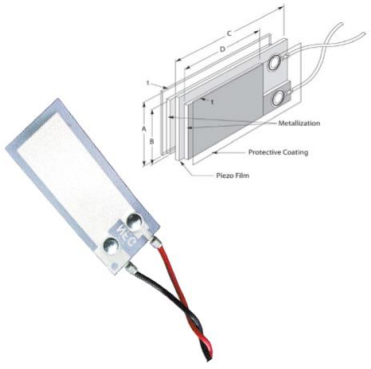

Figure 2.7 - Structure of DT Series Elements with lead attachment [20]

2.4.4 LDT Series Elements with Lead Attachment and Lamination

This sensor known as LDT, where 'L' stands for 'laminated' sensor. Typically, a 125µm polyester layer is laminated to a 28 µm or 52µm piezo film element. When used in a 'bending' mode, plated film elements generate much higher voltage output when flexed than a non-laminated DT elements series. The neutral axis is in the laminate is more strained when flexed and the capacitance of this sensor is proportional to the area and inversely proportional to the thickness of the element.

Piezo film sensors LDT elements are available in a variety of lead attachment options and in order to increase sensitivity small amounts of weight can be added. The LDT0-028K and LDTM-028K models (where M stands for the added mass), with solder tabs can be soldered directly to a PCB with a reasonable level of care. Piezo film cannot resist high temperatures (>80°C), so some precautions must be adopted in order during the soldering process.

Applications for this sensor include beam-type vibration sensors for vehicle alarms and solid state switches for counters and momentary closing type switches. A structure representation of the LDT sensor is shown in figure 2.8.

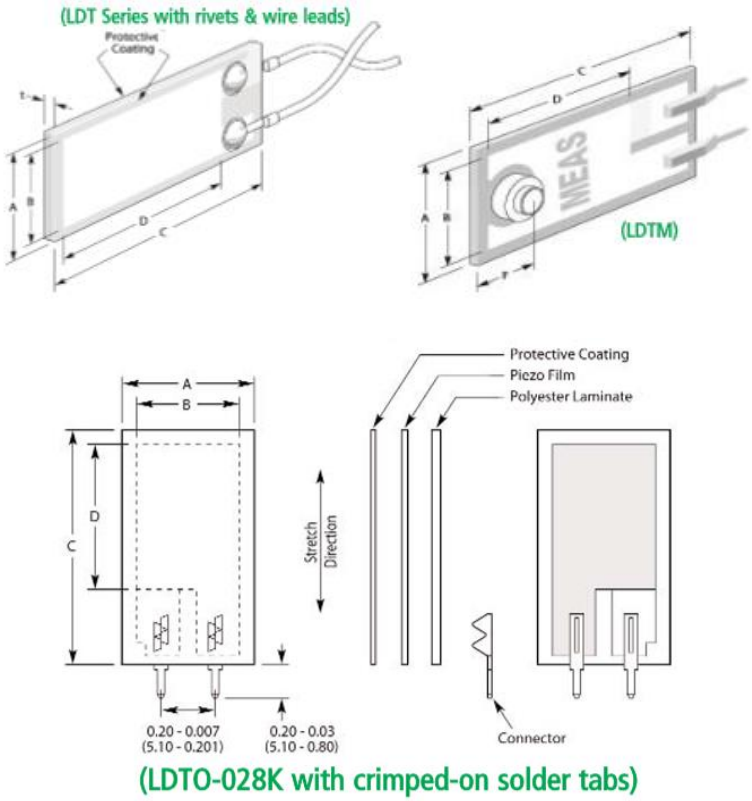

Figure 2.8 - Structure of LDT Series Elements with Lead Attachment and Lamination [20]

2.4.5 FDT Series Elements with Lead Attachment

This sensor is known as FDT, where “F” stands for ‘Flexible Leads’. These are rectangular elements of piezo film with silver ink screen printed electrodes. Rather than making the lead attachment near the sensor, the piezo polymer tail extends from the active sensor area as flex circuit material with offset traces. This gives a very flat, flexible lead, with a connector at the end, as represented in Figure 2.9.

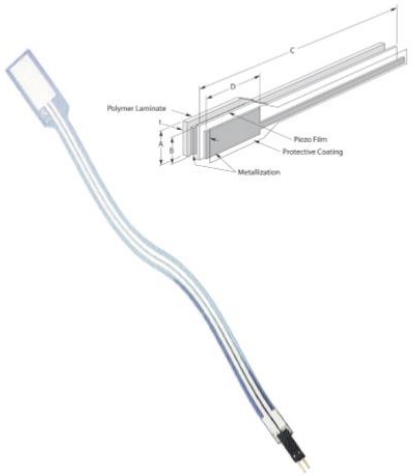

Figure 2.9 - structure of FDT Series Elements with Lead Attachment [20]

2.4.6 SDT Shielded piezo sensors element with shielded cable

The SDT Series sensors are ‘covered sensors’. These piezo film sensors consists of a rectangular element of piezo film with a molded plastic housing and 18” of coaxial cable. The film element, screen printed with silver ink, is bent over on itself, given a self-shielding of the transducer area. This is important in applications in high electromagnetic interference (EMI) environments [20]. A structure representation of the SDT sensor is shown in Figure 2.10.

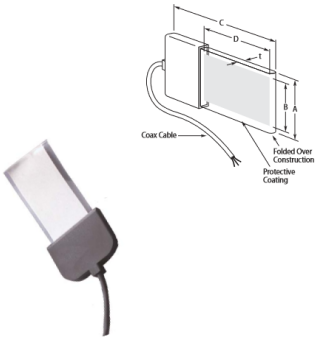

Figure 2.10 - Structure of SDT shielded piezo sensors element with shielded cable[20]

2.4.7 Piezo film solid state switches

Piezo film's capabilities to generate a high voltage output under bending strain, combined with its rugged form factor, make it an ideal for solid state switches. Rather than using a switch contact closure, the piezo film generates a pulse which is detected by electronics components. A structure representation of this sensor is shown in figure 2.11.

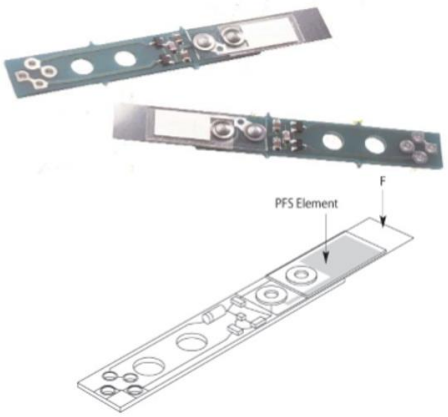

Figure 2.11 – Structure of Piezo Film Solid State Switches [20]

2.4.8 Piezo polymer coaxial cable

Piezo cable is a form of piezo polymer sensors. Designed as a coax cable, the piezo polymer is the "dielectric" between the centre core and the outer braid. When the cable is compressed or stretched, a charge or voltage is generated proportional to the stress. A structure representation of this sensor is shown in figure 2.12.

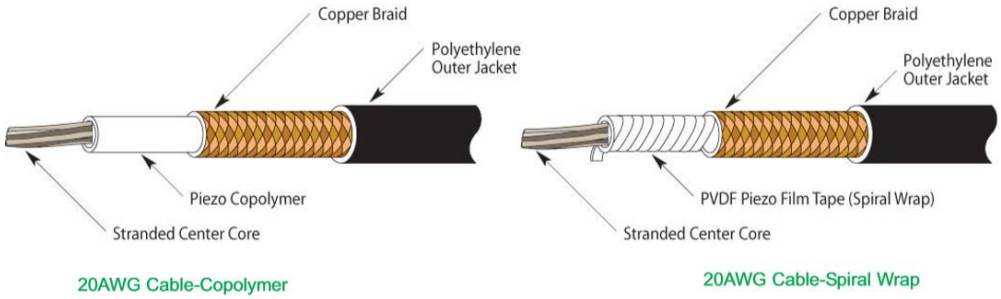

Figure 2.12 - Structure of Piezo Polymer Coaxial Cable [20]

2.5 Conclusion

The study of energy harvesting sources is relevant to understand under which context can be an energy harvester sensor be applied. In addition, the performed research and analysis on different piezoelectric actuators and sensors, allowed to support the choice of QP20W sensor used in this work, where the vibrational energy source is also considered.

CHAPTER 3

Piezoelectric film mathematic models

3. Piezoelectric film mathematic models

There are two different application for the cantilever mathematical model described by, 33 mode and 31 mode [30].

In Figure 3.1 can be observed the difference between theses modes in which piezoelectric materials can be used for harvesting applications. If we used the piezoelectric film in d33 mode is used, it means that both voltage and stress are acting in direction 3 , both of them are parallel to one another, meanwhile applied mechanical stress is vertical to the piezoelectric energy harvester (PEH) electrodes. An example of such PEH operation mode is piezoelectric stacks or wireless sensor nodes.

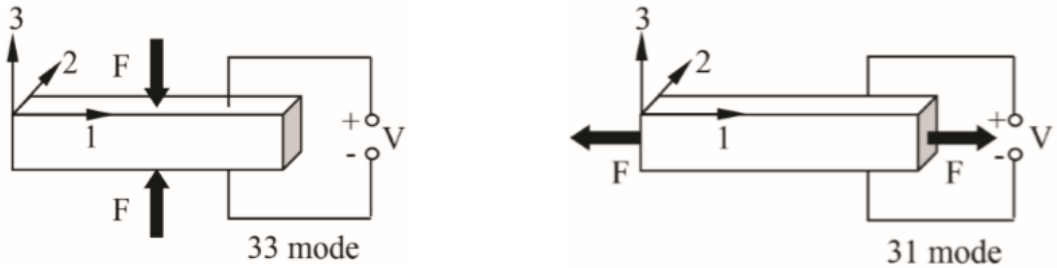

Figure 3.1 - Illustration of d33 mode and d31 mode operation for piezoelectric materials [30]

On the other hand, if piezoelectric film in d31 mode is used, in this case the voltage acts in direction 3 and mechanical stress acts in direction 1 (they are vertical to one another) and mechanical stress is parallel to PEH electrodes. Typical examples of PEH operation mode are vibration energy harvesting sensors.

There are different ways to modulate piezoelectric film [22,24,30]. In this work vibroimpacting piezoelectric energy harvester mathematical model (VIEPH) is addressed, because his working principle is line with the QP20W selected sensor.

3.1 Vibroimpacting piezoelectric energy harvester model

A 2D finite element (FE) model of vibroimpacting piezoelectric energy harvester (VIPEH) was developed with Comsol Multiphysics software. Figure 3.2 and Table 3.1 provide principal scheme and geometry data of developed transducer - cantilever beam of stainless steel

covered by piezoelectric layer (of PZT, PVDF or PMN-PT), operating in transverse (d31) mode. Modelling was performed with Lagrange-quadratic. Where Lagrange-quadratic or Lagrange polynomials are used for polynomial interpolation, i.e, for "approximating the values of a function". For a given set of points (x_j, y_j) with two x_j equal values, the Lagrange polynomial is the lowest degree polynomial that assumes, at each value x_j the corresponding value y_j, i.e., the functions are coincident at each point [31]. Boundary conditions are settled to represent electrodes enveloping piezoelectric material and structure clamping.

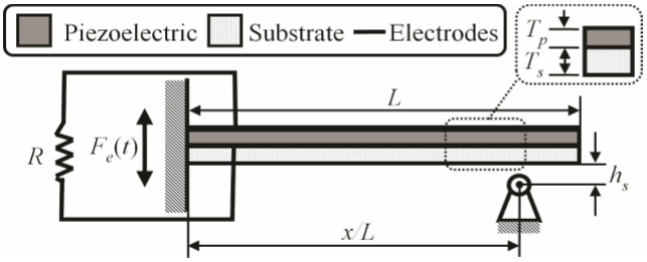

Figure 3.2- Principal scheme of developed FE model of PEH [22]

The model parameters are detailed in table 3.1.

Table 3.1 - VIEPH model parameters [22]

Parameter	Value	Description
Ls	100 mm	Substrate length
Lp	100 mm	Piezoelectric layer length
Ts	1 mm	Substrate thickness
Tp	0.2 mm	Piezoelectric layer thickness
Ws	10 mm	Substrate width
Wp	10 mm	Piezoelectric layer width
A	1.0*g	Applied excitation acceleration
Rsc	100 Ω	Connected resistor load, corresponding to closed circuit conditions
Roc	1 MΩ	Connected resistor load, corresponding to open circuit conditions
Fe	*	Applied excitation frequency (corresponding to 1st resonant system frequency
hs	2 µm	Stopgap size at the support location
$CvdW$	1 x10^{-32}	Adhesion constant

Piezoelectric energy harvester PEH dynamics is described by (3.1) equation of motion presented in a general matrix form [22]:

$$[M]\{\ddot{Z}\}+[C]\{\dot{Z}\}+[K]\{Z\}=\{Q(t,Z,\dot{Z})\} \quad (3.1)$$

Where $[M]$, $[C]$, $[K]$, are mass, damping and stiffness matrices of the harvester, respectivel; $\{Z\},\{\dot{Z}\},\{\ddot{Z}\}$ are displacement, velocity and acceleration vectors, respectively; while $\{Q(t,Z,\dot{Z})\}$vector represents the sum of external forces acting on the PEH .

To define piezoelectric effects, the following considerations and constitutive piezoelectric equations were used in the FE model [23]. When piezoelectric material is subjected to stress T, it produces polarization P, which is function of stress (direct piezoelectric effect), given by equation (3.2).

$$P=dT \tag{3.2}$$

In contrast, when electric field E is applied across electrodes of piezoelectric material, it produces strain S, which is function of electric field (inverse piezoelectric effect) , given by (3.3).

$$S=dE \tag{3.3}$$

For a dielectric substance, the relationship between electrical displacement D and electric field strength *E* is given by (3.4).

$$D=\varepsilon_0 E+P \tag{3.4}$$

Where ε_0 is the dielectric permittivity of vacuum and P being the material polarization due to applied field. From these relationships, with electric field E and stress T as independent variables, the two constitutive piezoelectric equations are given by (3.5) and (3.6).

$$S=s^E\ T+dE \tag{3.5}$$

$$D=dT+\varepsilon^T\ E \tag{3.6}$$

Where S is the strain tensor; T is the stress tensor; E is the electric field vector; D is the electric displacement vector; s is the elastic compliance matrix when subjected to a constant electric field; d is the piezoelectric constant matrix and ε is the permittivity measured at a constant stress.

Since phenomenon of piezoelectricity is anisotropic (i.e depends on many variables such as the material of them. Thickness and direction of mechanical force and stress), electric field E

and electrical displacement D are represented in vector magnitudes, while stress T and stain S are given in symmetrical tensile magnitudes by (3.7) and (3.8).

$$S_i = S_{ij}^E T_j + d_{mi} E_m \tag{3.7}$$

$$S_n = d_{nj} T_j + \varepsilon_{nm}^T E_m \tag{3.8}$$

where $m, n = 1,2,3;$ and $i, j = 1,2,..,6$.

These equations can be as well represented in matrix form, given by (3.9) and (3.10), respectively:

$$\begin{bmatrix} S1 \\ S2 \\ S3 \\ S4 \\ S5 \\ S6 \end{bmatrix} = \begin{bmatrix} S_{11}^E & S_{12}^E & S_{13}^E & 0 & 0 & 0 \\ S_{12}^E & S_{11}^E & S_{13}^E & 0 & 0 & 0 \\ S_{13}^E & S_{13}^E & S_{33}^E & 0 & 0 & 0 \\ 0 & 0 & 0 & S_{44}^E & 0 & 0 \\ 0 & 0 & 0 & 0 & S_{44}^E & 0 \\ 0 & 0 & 0 & 0 & 0 & 2(S_{11}^E - S_{12}^E) \end{bmatrix} \begin{bmatrix} T1 \\ T2 \\ T3 \\ T4 \\ T5 \\ T6 \end{bmatrix} + \begin{bmatrix} 0 & 0 & d_{31} \\ 0 & 0 & d_{31} \\ 0 & 0 & d_{31} \\ 0 & d_{31} & 0 \\ d_{31} & 0 & 0 \\ 0 & 0 & 0 \end{bmatrix} \begin{bmatrix} E1 \\ E2 \\ E3 \end{bmatrix} \tag{3.9}$$

$$\begin{bmatrix} D1 \\ D2 \\ D3 \end{bmatrix} = \begin{bmatrix} 0 & 0 & 0 & 0 & d_{15} & 0 \\ 0 & 0 & 0 & d_{15} & 0 & 0 \\ d_{31} & d_{31} & d_{31} & 0 & 0 & 0 \end{bmatrix} \begin{bmatrix} T1 \\ T2 \\ T3 \\ T4 \\ T5 \\ T6 \end{bmatrix} + \begin{bmatrix} \varepsilon_{11} & 0 & 0 \\ 0 & \varepsilon_{11} & 0 \\ 0 & 0 & \varepsilon_{33} \end{bmatrix} \begin{bmatrix} E_1 \\ E_2 \\ E_3 \end{bmatrix} \tag{3.10}$$

In order to simulate PEH operating in vibro-impacting mode, a viscoelastic - adhesive contact formulation was implemented into the FE model of PEH. This formulation is based on Kelvin-Voigt rheological model. This means that the springs and dampers can be putted together to develop mathematical models of viscoelastic behaviour. In a Maxwell model, the spring and the damper are in series, but they are in parallel in the Kelvin-Voigt model. The construction of Kelvin-Voigt rheological models can be obtained through joining the simplest Kelvin-Voigt and Maxwell models in various combinations [32], represented by linear spring connected in parallel with linear damper, where this coupling element is defined by stiffness Kp and damping Cp. Additionally, adhesion-related parameter C_{vdW} is introduced, which allows taking into account Van der Waals forces acting at the micro-scale before mechanical contact actually occurs. Therefore, the proposed contact model may be used for simulations of both macro- and micro-scale energy harvesting devices. Dynamics of the VIPEH is given by (3.11) and (3.12).

$$[M]\{\ddot{Z}\} + [C]\{\dot{Z}\} + [K]\{Z\} =$$

$$= \begin{cases} \{F(t)\} + \{F_S(t)\}, & if\ z_{l_s}(t) < h_{s-\xi_0} \vee P_{l_s}\left(\dot{z}_{l_s}, z_{l_s}, t\right) \geq 0; \\ \{F(t)\} + \{F_S(t)\} + \{P_c(z, \dot{z}, t)\}, & if\ z_{l_s}(t) \geq h_{s-\xi_0} \wedge P_{l_s}\left(\dot{z}_{l_s}, z_{l_s}, t\right) < 0; \end{cases} \quad (3.11)$$

$$\{F_{lS}(t)\} = \begin{cases} \frac{C_v dW}{\left[h_s - z_{l_s}(t)\right]^3}, & if\ z_{l_s}(t) < h_{s-\xi_0} \vee P_{l_s}\left(\dot{z}_{l_s}, z_{l_s}, t\right) \geq 0; \\ \frac{C_v dW}{\xi_0^3}, & if\ z_{l_s}(t) \geq h_{s-\xi_0} \wedge P_{l_s}\left(\dot{z}_{l_s}, z_{l_s}, t\right) < 0; \end{cases} \quad (3.12)$$

Where $\{\dot{z}(0)\} = \{\dot{z^0}\}$, $\{z(0)\} = \{z^0\}$ and [M], [C], [K] are mass, damping and stiffness matrices of PEH respectively; $\{\dot{Z}\}$, $\{\ddot{Z}\}$ are velocity and acceleration vectors, respectively, $\{z^0\}$ is displacement at t=0; $\{\dot{z^0}\}$ is velocity at time point t = 0 ; $\{F(t)\}$ is the external forces vector of acting on PEH (in this case this is base excitation); $\{F_S(t)\}$ is the vector representing existing influence of Van der Waals forces and $\{P_c(z, \dot{z}, t)\}$ is the vector of nonlinear interaction in the contact pair.

The developed contact model is given by (3.13) and (3.14).

$$C_v dW = \frac{A_H A_C}{6\pi} \quad (3.13)$$

$$P_{l_s}\left(\dot{z}_{l_s}, z_{l_s}, t\right) = -K_P \left[z_{l_s}(t) - (h_{s-\xi_0}) \right] - C_P \dot{z}_{l_s}(t), \quad (3.14)$$

Where $z_{l_s}(t)$, $\dot{z}_{l_s}(t)$ are respectively displacement and velocity of PEH surface point; hs is stopgap; $\xi 0$ is the distance between surfaces when it is assumed that mechanical contact has occurred (~1 nm); K_P and C_P are stiffness and damping of the coupling element, respectively; A_H is Hamaker's constant; A_C is the contact area and P_{l_s} is the contact pair's nonlinear interaction force at contact point (l_s is the contact point position along longitudinal axis, measured from the clamped end, where l=0). Developed contact model was introduced into the FE model of PEH as a transverse force acting on selected point located on the bottom edge of the PEH cantilever. The model allows variation of both vertical and horizontal position of the "virtual" support with respect to the transducer surface.

3.2 Direct and inverse effect of piezoelectricity

Direct effect of piezoelectricity appears when a mechanical stress applied on a material produces an electrical polarization. On the other hand, inverse effect of piezoelectricity appears when an applied electric field in a material produces dimensional changes and stresses within a material. For example, ultrasonic transceivers for marine sonar ultrasound systems for non-invasive biomedical imaging and the needles of record players microphones are some applications of the inverse effect.

Because is considered relevant considering the application of both of direct and inverse effect to the mathematical model, those effects are addressed [24].

The direct effect of piezoelectricity can be described by the general equation and given by (3.15).

$$D = dT + \varepsilon E \tag{3.15}$$

Where D is the electrical polarization (C/m^2), T is the stress vector (N/m^2), d is the piezoelectric Coefficient Matrix, ε is electrical permittivity matrix (F/m) and E is the electric field vector (V/m).

These equations can be represented in a matrix form given by (3.16).

$$\begin{bmatrix} D1 \\ D2 \\ D3 \end{bmatrix} = \begin{bmatrix} d_{11} & d_{12} & d_{13} & d_{14} & d_{15} & d_{16} \\ d_{21} & d_{22} & d_{23} & d_{24} & d_{25} & d_{26} \\ d_{31} & d_{32} & d_{33} & d_{34} & d_{35} & d_{36} \end{bmatrix} \begin{bmatrix} T1 \\ T2 \\ T3 \\ T4 \\ T5 \\ T6 \end{bmatrix} + \begin{bmatrix} \varepsilon_{11} & \varepsilon_{12} & \varepsilon_{13} \\ \varepsilon_{21} & \varepsilon_{22} & \varepsilon_{23} \\ \varepsilon_{31} & \varepsilon_{23} & \varepsilon_{33} \end{bmatrix} \begin{bmatrix} E_1 \\ E_2 \\ E_3 \end{bmatrix} \tag{3.16}$$

The direct effect of piezoelectricity can be simplified, in the absence of an external electric field (i.e. E=0), resulting in the equations given by (3.17-3.18).

$$D = dT \tag{3.17}$$

$$\begin{bmatrix} D1 \\ D2 \\ D3 \end{bmatrix} = \begin{bmatrix} d_{11} & d_{12} & d_{13} & d_{14} & d_{15} & d_{16} \\ d_{21} & d_{22} & d_{23} & d_{24} & d_{25} & d_{26} \\ d_{31} & d_{32} & d_{33} & d_{34} & d_{35} & d_{36} \end{bmatrix} \begin{bmatrix} T1 \\ T2 \\ T3 \\ T4 \\ T5 \\ T6 \end{bmatrix} \tag{3.18}$$

The inverse effect of piezoelectricity can be described by the general equation and given by (3.19).

$$\boldsymbol{S}=ST+dE \tag{3.19}$$

Where $\boldsymbol{S}$ is strain vector; S is the compliance matrix, T is the stress vector (N/m^2), d is piezoelectric coefficient matrix and E is electric field vector (V/m).

Equation (3.19) can be represented in a matrix form given by (3.20).

$$\begin{bmatrix} S_1 \\ S_2 \\ S_3 \\ S_4 \\ S_5 \\ S_6 \end{bmatrix} = \begin{bmatrix} S_{11} & S_{12} & S_{13} & S_{14} & S_{15} & S_{16} \\ S_{21} & S_{22} & S_{23} & S_{24} & S_{25} & S_{26} \\ S_{31} & S_{32} & S_{33} & S_{34} & S_{35} & S_{36} \\ S_{41} & S_{42} & S_{43} & S_{44} & S_{45} & S_{46} \\ S_{51} & S_{52} & S_{53} & S_{54} & S_{55} & S_{56} \\ S_{61} & S_{62} & S_{63} & S_{64} & S_{65} & S_{66} \end{bmatrix} \begin{bmatrix} T1 \\ T2 \\ T3 \\ T4 \\ T5 \\ T6 \end{bmatrix} + \begin{bmatrix} d_{11} & d_{21} & d_{31} \\ d_{12} & d_{22} & d_{32} \\ d_{13} & d_{23} & d_{33} \\ d_{14} & d_{24} & d_{34} \\ d_{15} & d_{25} & d_{35} \\ d_{16} & d_{26} & d_{36} \end{bmatrix} \begin{bmatrix} E_1 \\ E_2 \\ E_3 \end{bmatrix} \tag{3.20}$$

The inverse effect of piezoelectricity can be simplified accordingly to (3.21) and (3.22), if there is no additional mechanical stress present (i.e. T=0). Where strain is related the electric field by equation (3.21), represented in matrix form in (3.22).

$$S = d\,E \tag{3.21}$$

$$\begin{bmatrix} S_1 \\ S_2 \\ S_3 \\ S_4 \\ S_5 \\ S_6 \end{bmatrix} = \begin{bmatrix} d_{11} & d_{21} & d_{31} \\ d_{12} & d_{22} & d_{32} \\ d_{13} & d_{23} & d_{33} \\ d_{14} & d_{24} & d_{34} \\ d_{15} & d_{25} & d_{35} \\ d_{16} & d_{26} & d_{36} \end{bmatrix} \begin{bmatrix} E_1 \\ E_2 \\ E_3 \end{bmatrix} \tag{3.22}$$

Where the units of the piezoelectric constant, *dij*, are the units of electric displacement over the unit of the stress.

Therefore the piezoelectric constant is a good way to measure the intensity of the piezoelectric effect, since it can be related in terms of Columns generated, per Newton applied.

Some values of piezoelectric constant for some different material are shown in table 3.2.

Table 3.2 - *d33* piezoelectric value

Piezo material	**structure**	***d33* value**
Zinc oxide *(ZnO)*	sputtered thin film (STF)	*246 pC/N*
Lead zirconate titanate (*PZT*)	ceramic bulk, or STF	*110 pC/N*
Quartz	- bulk single crystal	*2.33 pC/N*
Polyvinylidene fluoride (*PVDF*)	polymer	*1.59 pC/N*

3.3 Unimorph piezoelectric film modelling using Erturk and Inman theory

Before addressing the mathematical model some description of the unimorph piezoelectric film is presented. Considering an example of a unimorph energy harvester, which is depicted in Figure 3.3.

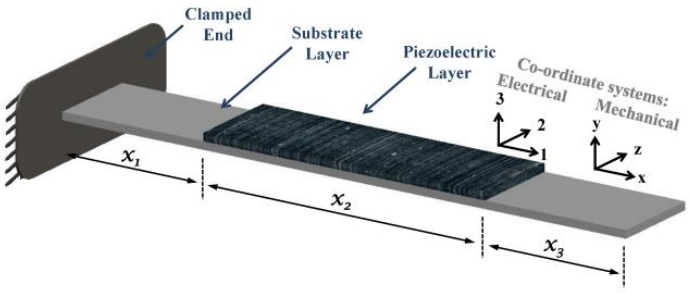

Figure 3.3- Example of a unimorph energy harvester [4]

In Figure 3.3, x_2 refers to the piezoelectric material length, x_1 is the offset distance of piezoelectric material from the clamped end and x_3 is the distance from the end of the piezoelectric material to cantilever tip. Upper and lower surfaces of the piezoelectric layer are fully coated with electrode material.

The corresponding mathematical model of the unimorph piezoelectric film is detailed in 3.3.1

3.3.1 Mechanical equation of motion

The unforced transverse vibration of an undamped beam is given by equation (3.23),[25].

$$\frac{d^2M(x,t)}{d_{x^2}} + m(x)\frac{d^2\omega(x,t)}{d_{t^2}} = 0\ , \tag{3.23}$$

Where $\omega(x,t)$ is the transverse deflection, $M(x,\ t)$ is the internal moment of the beam cross-section and $m(x)$ is the mass per unit length. In this model is considered an Euler-Bernoulli beam whereby rotary inertia effects and shear deformation are ignored by assuming the beam is long and slender [25]. The conventional method for transferring vibrational energy to the beam structure is through base excitation [25]. For the purposes of analysis it is convenient to express the flexural displacement, $\omega(x,t)$, of the beam accordingly with (3.24).

$$\omega(x,t) = \omega_{rel}(x,t) + \omega_b(x,t) \tag{3.24}$$

Where $\omega_{rel}(x,t)$is the beam displacement relative to the base and $\omega_b(x,t)$ the base displacement. The following piezoelectric constitutive equations (3.25-3.26) are used to describe the electromechanical coupling properties for the piezoelectric material [1].

$$\sigma_{11}^{p} = E_p\, \varepsilon_{11}^{p} - E_p\, d_{31}\, (E_{field})_3 \quad (3.25)$$

$$D_3 = E_p\, d_{31} \varepsilon_{11}^{p} + \varepsilon_{33}^{S}\, (E_{field})_3 \quad (3.26)$$

Where σ is the stress and D the electric displacement. E_p , ε and E_{field} represents the Young's modulus, strain and electric field strength, respectively; d31 is the piezoelectric material constant and ε_{33}^{S} is the permittivity at constant strain .

Assuming the electric field is uniform throughout the constant piezoelectric material thickness, t_p, then $(E_{field})_3$ (t) given by (3.27).

$$\left(E_{field}\right)_3(t) = -\frac{V(t)}{t_p} \quad (3.27)$$

Where $V(t)$ is the voltage across the piezoelectric layer electrodes. The constitutive equation for the substrate material is used to relate stress and strain and is given by (3.28).

$$\sigma_{11}^{p} = E_s\, \varepsilon_{11}^{s} \quad (3.28)$$

Where, subscript '*s*' refers to the substrate material.

The internal moment, $M(x,t)$, which appears in (3.23) can be expressed as (3.29).

$$M(x,t) = -\int_{h_a}^{h_b} \sigma_{11}^{s}\, b_s\, y\, dy - \int_{h_b}^{h_c} \sigma_{11}^{p}\, b_p\, y\, dy \quad (3.29)$$

Where $b_s$and b_p are the widths of the substrate and piezoelectric layers, which are assumed to be constant along the beam length. The terms h_a, h_b and h_c are defined in figure 3.4 and are dependent on the position of the neutral axis, *y,* where the position of the neutral axis is given by (3.30).

$$\bar{y} = \frac{t_s{}^2\, b_s + t_p{}^2\, n\, b_p + 2\, t_s t_p\, n\, b_p}{2(\, t_s\, b_s + t_p\, n\, b_p\,)} \quad (3.30)$$

Where *n* is the constant ratio of the piezoelectric Young's modulus to the substrate Young's modulus (E_p/E_s).

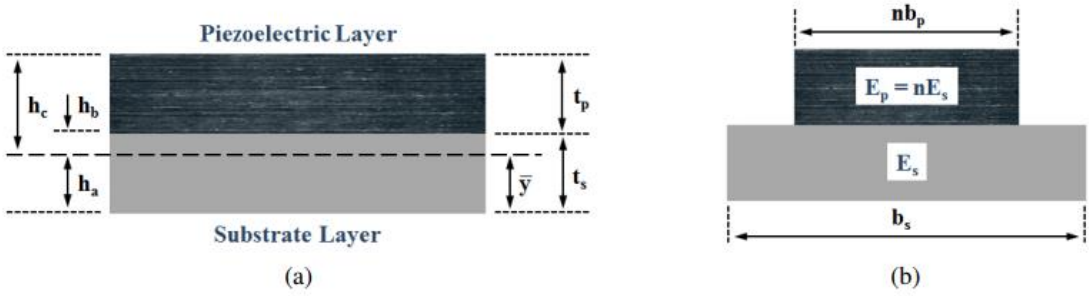

Figure 3.4- Cross-sectional view of unimorph energy harvester [4].

The strain in the beam can be approximated to the equation given by (3.31).

$$\varepsilon(x,t) = -y\frac{d^2\omega_{rel}(x,t)}{d_{x^2}} \tag{3.31}$$

Where y is the distance from the neutral axis. Using (3.25), (3.28) and (3.31) in (3.29), the internal moment can be expressed as (3.32).

$$M(x,t) = E_s I_s + \frac{d^2\omega_{rel}(x,t)}{d_{x^2}} + E_p I_p + \in V(t) \tag{3.32}$$

Where I_s and I_p are expressions for the second moment of area and which is an electromechanical coupling term given by (3.33– 3.35), respectively.

$$I_s = \frac{b_s}{3}\left[(t_s - \bar{y})^3 - (-\bar{y})^3\right] \tag{3.33}$$

$$I_p = \frac{b_p}{3}\left[(t_p + t_s - \bar{y})^3 - (t_s - \bar{y})^3\right] \tag{3.34}$$

$$\in = -\frac{E_p\, b_p\, d_{31}}{2\, t_p}\left[(t_p + t_s - \bar{y})^2 - (t_s - \bar{y})^2\right] \tag{3.35}$$

As opposed to the Erturk and Inman model [26], Heaviside functions are introduced and carried throughout derivation. Since parametric studies on geometry will affect the length and position of piezoelectric material, Heaviside functions are used to limit the contribution of the finite length piezoelectric layer on the overall moment [25]. Using this approach the internal moment can be given by (3.36).

$$M(x,t) = EI(x)\frac{d^2\omega_{rel}(x,t)}{d_{x^2}} + \in V(x,t) \tag{3.36}$$

Where $\omega_{rel}(x,t)$ is the beam displacement relative to the base and $\in$ is the electromechanical coupling term. $EI\,(x)$ is the flexural rigidity defined by (3.37) and $V(x,t)$ is defined by (3.38).

$$EI\,(x) = E_S\,I_S + E_P\,I_P\,[H(x - x_1) - H(x - x_1 - x_2)] \quad (3.37)$$

$$V(x,t) = V(t)\,[H(x - x_1) - H(x - x_1 - x_2)] \quad (3.38)$$

Where $V\,(t)$ is the voltage across the piezoelectric layer electrodes and $H(x)$ are Heaviside functions.

A similar approach can be used to represent the mass term present in (3.23), and using (3.23-3.36) can be expressed as (3.39).

$$\frac{d^2}{d_{x^2}}\left[EI\,(x)\,\frac{d^2\omega_{rel}(x,t)}{d_{x^2}} + \in V\,(x,t)\right] + m(x)\frac{d^2\omega_{rel}(x,t)}{d_{t^2}} = m(x)\frac{d^2\omega_b(x,t)}{d_{t^2}} \quad (3.39)$$

Where $m(x)$ is the mass per unit length defined by (3.40).

$$m(x) = \rho_s\,A_s + \rho_s\,A_s\,[H(x - x_1) - H(x - x_1 - x_2)] \quad (3.40)$$

Where $H(x)$ are Heaviside functions, ρ_s is the substrate material density and A_s is the substrate layer cross-sectional area.

The mechanical behaviour of a piezoelectric beam is mathematically represented by (3.39) and can be analysed using classical modal analysis techniques. Where classical modal analysis is the study of the dynamic properties of systems in the frequency domain. This study is made by with a SIMO (single-input, multiple-output) approach, i.e, one excitation point, and then the response is measured at many other points[33]. Using this approach the beam deflection, $\omega_{rel}(x,t)$, is expressed as an infinite sum of products of normalised eigenvectors, $W_r(x)$, and time dependant generalised co-ordinates, $\eta_r\,(t)$ given by (3.41).

$$\omega_{rel}(x,t) = \sum_{r=1}^{\infty} W_r(x)\,\eta_r\,(t) \quad (3.41)$$

Where index 'r' refers the mode number. Using (3.41) and replacing in (3.39) results in (3.42).

$$\frac{d^2}{d_{x^2}}\left[EI(x)\sum_{r=1}^{\infty} W_r''(x)\,\eta_r\,(t) + \in V(x,t)\right] + m(x)\sum_{r=1}^{\infty} W_r(x)\,\ddot{\eta}_r(t) = m(x)\,\ddot{\omega}_b(t) \quad (3.42)$$

In (3.42)(") refers to the second derivative with respect to longitudinal position, and ($\ddot{}$) refers to the second derivative with respect to time.

As a result of multiplying (3.42) by $W_q(x)$ and integrating over the beam length, (3.43) is obtained.

$$\ddot{\eta}_q(t) + \omega_q{}^2 \eta_q(t) + \in \int_0^L W_q(t) \frac{d^2V(x,t)}{d_{x^2}} dx = \ddot{\omega}_b(t) \int_0^L m(x) W_q(x)\, dx \quad (3.43)$$

Where the orthogonality conditions given by (3.44 – 3.45) have been used.

$$\int_0^L W_q(x)\, m(x)\, W_r(x)\, dx = \delta_{rq}\,,\ r,q = 1,2,3 \quad (3.44)$$

$$\int_0^L W_q(x)(EI(x))'' W_r''(x))\, dx = \omega_q{}^2\, \delta_{rq}\,,\ r,q = 1,2,3 \quad (3.45)$$

Where $W_q(x)$and $W_r(x)$ are normalised eigenvectors, *m(x)* is the mass per unit length,δ_{rq} is the Kronecker delta function which is unitary when r = q, and zero otherwise, and ω_q is the undamped natural frequency of the q^{th} mode.

The voltage term in (3.43) can be manipulated by introducing the Dirac function [27], δ(x), as the derivative of the Heaviside function resulting in (3.46).

$$\in \int_0^L W_q(x) \frac{d^2V(x,t)}{d_{x^2}} dx = \in V(t)\, [W_q'(x_1 + x_2) - W_q'(x_1)] \quad (3.46)$$

Replacing (3.46) in (3.43), results the function given by (3.47)

$$\ddot{\eta}_q(t) + \omega_q{}^2 \eta_q(t) + \in V(t)\, [W_q'(x_1 + x_2) - W_q'(x_1)] = \ddot{\omega}_b(t) \int_0^L W_q(x)\, m(x)\, dx \quad (3.47)$$

Where (3.47) provides the modal response of a piezoelectric beam subjected to base excitation. Note that damping is currently not present in this equation and its inclusion is detailed in 3.3.2

3.3.2 Proportional damping

Some form of damping must be included in the system due to the presence of energy dissipation in all real situations. It is mathematically convenient to assume proportional damping [28], where damping matrix can be expressed as:

$$[C] = \alpha[M] + \beta[K] \quad (3.48)$$

Where α and β are constants and can be obtained from experimental data. Consider the damped equation of motion for a beam is given by (3.49) [29].

$$[M]\,\ddot{\omega}_{rel}+[C]\,\dot{\omega}_{rel}+[K]\,\omega_{rel}=F(t) \tag{3.49}$$

Where $F(t)$ is an arbitrary force. Using (3.41) for the beam deflection in (3.49) results in (3.50).

$$[M]\sum_{r=1}^{\infty} W_r(x)\;\ddot{\eta}_r\,(t)+[C]\sum_{r=1}^{\infty} W_r(x)\;\dot{\eta}_r\,(t)+[K]\sum_{r=1}^{\infty} W_r(x)\;\eta_r\,(t)=F(t) \tag{3.50}$$

Modal decoupling and the modal orthogonality conditions (3.44 – 3.45) can be used on (3.50) along with (3.48), allowing (3.50) to be written accordingly with (3.51).

$$\ddot{\eta}_q\,(t)+(\alpha+{\omega_q}^2\,\beta)\,\dot{\eta}_q\,(t)+{\omega_q}^2\,\eta_q(t)=W_q(x)\,F(t) \tag{3.51}$$

Where $\eta_q(t)$ is generalised modal co-ordinate , α is the 1st constant for proportional damping β is the 2nd constant for proportional damping, ${\omega_q}^2$ is the natural frequency, $W_q(x)$ is normalised eigenvectors and $F(t)$ is an arbitrary force .

If W_q(x) is written in the matrix form, results the equation given by (3.52 – 3.53).

$${W_q}^T\,[M]W_q=1 \tag{3.52}$$

$${W_q}^T\,[M]W_q={\omega_q}^2 \tag{3.53}$$

Introducing of the modal damping ratio, γ [29], results in the relationship given by (3.54).

$$(\alpha+{\omega_q}^2\,\beta)=2\gamma_q\,\omega_q \tag{3.54}$$

Proportional damping is useful because it incorporates changes in mechanical damping magnitude with changes in energy harvester geometry due to differences in the fundamental frequency of configurations. Introducing modal damping in (3.47) allows the complete modal behaviour of the energy harvester to be predicted using (3.55).

$$\ddot{\eta}_q(t)+2\gamma_q\omega_q\dot{\eta}_q(t)+{\omega_q}^2\eta_q(t)+\epsilon V(t)[\,W_q'(x_1+x_2)-W_q'(x_1)]= \\ =\ddot{\omega}_b\,(t)\int_0^L W_q\,(x)\;m(x)\,dx \tag{3.55}$$

Equation (3.55), which now includes a contribution from mechanical damping, will be used in conjunction with an electrical equation derived in 3.3.3 resulting in a fully describe electromechanical behaviour of a piezoelectric cantilever energy harvester.

3.3.3 Electrical equation

Considering that, initially the piezoelectric cantilever is connected to a load resistor, as shown Figure 3.5.

Using (3.27) and (3.31) in (3.26) the 2nd piezoelectric constitutive equation can be expressed as (3.56).

$$D_3(x,t) = -E_p\, d_{31}\, t_{pc} \frac{d^2 \omega_{rel}(x,t)}{d_{x^2}} - \frac{\varepsilon_{33}^S}{t_p} V(t) \qquad (3.56)$$

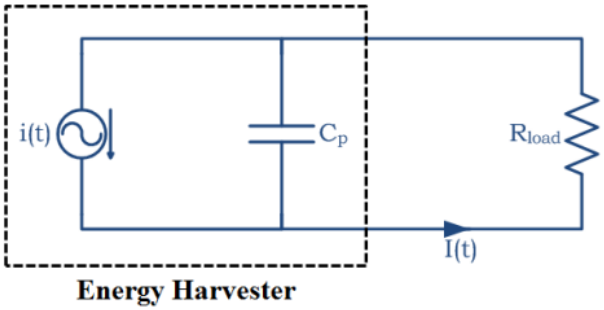

Figure 3.5- Electrical representation of energy harvester connected to a resistor[4].

Where E_p Young's modulus of piezoelectric material , t_{pc} is the distance between the neutral axis y, and the piezoelectric material centre , t_p is the Thickness of piezoelectric layer , ε_{33}^S is permittivity at constant strain and $d_{31}$is piezoelectric material constant .

The generated charge, $q(t)$, can be calculated using a form of Gauss's Law, by integrating electric displacement over the electrode area accordingly with (3.57).

$$q(t) = \iint_{A_e} D_3(x,t)\, dA_e \qquad (3.57)$$

Where $q(t)$ is the generated charge, $D_3(x,t)$ is the 2nd piezoelectric constitutive law and A_e is the electrode area.

The current generated by the energy harvester $i(t)$ is the time derivative of charge and composed by a contribution from vibratory beam motion and static capacitance of the piezoelectric material and is given by (3.58).

$$i(t) = -\int_{x_1}^{x_1+x_2} E_p\, d_{31}\, t_{pc}\, b_p \frac{d^3 \omega_{rel}(x,t)}{d_{x^2}} dx - C_p \frac{dV(t)}{dt} \qquad (3.58)$$

Where b_p is the piezoelectric layer width and C_p is the piezoelectric internal capacitance

given by (3.59).

$$C_p = \frac{\varepsilon_{33}^{S} b_p x_2}{t_p} \tag{3.59}$$

As previously mentioned, the harvester is connected to a load resistor, R_{load} and in this case Ohm's Law can be used in conjunction with (3.41) and (3.58) to obtain the differential equation for voltage generated given by (3.60).

$$C_p \frac{dV(t)}{dt} + \frac{V(t)}{R_{load}} = \sum_{q=1}^{\infty} -E_p d_{31} t_{pc} b_p \left[\frac{dW_{q(x)}}{dx}\right]_{x_1}^{x_1+x_2} \dot{\eta}_q(t) \tag{3.60}$$

Where R_{load} is the load resistance and η_q are the generalised modal coordinates. Equation (3.60) indicates that the voltage generated by the piezoelectric layer is dependent on the modal response of the beam, mode shape, internal capacitance, load resistance, and material mechanical and electric properties.

3.3.4 Modelling piezoelectric energy harvesting system connected to a storage capacitor

In this subchapter the mechanical and electrical equations (3.61-3.67) that represent the harvester system behaviour are addressed considering a capacitor as an energy storage. The considered system comprises an energy harvester, diode bridge for full wave rectification and a capacitor, as shown in Figure 3.6.

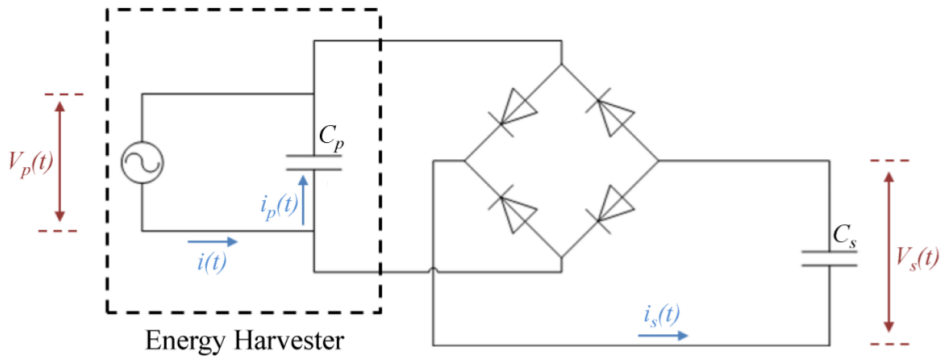

Figure 3.6 – Schematic of the charging circuit [4]

From equation (3.58) the current can be expressed as (3.61) :

$$i(t) = -E_p\, d_{31}\, t_{pc}\, b_p \left[\frac{dW_{1(x)}}{dx}\right]_{x_1}^{x_1+x_2} \dot{\eta}_q\,(t) \tag{3.61}$$

Where , E_p is the Young's modulus of piezoelectric material , $d_{31}$is piezoelectric material constant, t_{pc} is the distance between the neutral axis y and the piezoelectric material centre, b_p is the piezoelectric layer width, $\dot{\eta}_q(t)$ is the time derivative of the generalised modal co-ordinates , x_1 is the length from clamp to piezoelectric layer, $W_{1(x)}$ is the normalised eigenvectors and x_2 is the length of piezoelectric layer.

In (3.61) the modal co-ordinate $\dot{\eta}_q$ given by (3.62).

$$\ddot{\eta}_1\,(t) + +2\gamma_1\,\omega_1\dot{\eta}_1\,(t) + \omega_1{}^2\eta_1\,(t) = (Q_1 - R_1 V_p(t))\, e^{i\omega t} \tag{3.62}$$

Where Q_1 is the mechanical force, R_1 is the electromechanical coupling and γ_1 is the mechanical damping ratio

The i_p (t) current depends on the diode bridge operation and is given by (3.63-3.64).

$$i_p(t) = \begin{cases} i(t) & for\ V_p(t) < V_s(t) + 2V_{th} \\ i(t)\ \frac{C_p}{C_s+C_p} & for\ V_p(t)\ \geq V_s(t) + 2V_{th} \end{cases} \tag{3.63}$$

$$i_s(t) = \begin{cases} 0 & for\ V_p(t) < V_s(t) + 2V_{th} \\ i(t)\ \frac{C_s}{C_s+C_p} & for\ V_p(t)\ \geq V_s(t) + 2V_{th} \end{cases} \tag{3.64}$$

The voltages $\dot{V}_p$ and $\dot{V}_s$ are given by (3.65-3.66)

$$\dot{V}_p\,(t) = i_p(t) / C_p \tag{3.65}$$

$$\dot{V}_s\,(t) = i_s(t) / C_s \tag{3.66}$$

Equations (3.62-3.66) can be written in matrix in from given by (3.67).

$$\begin{bmatrix} \dot{\eta} \\ \ddot{\eta} \\ \dot{V}_p \\ \dot{V}_s \end{bmatrix} = \begin{bmatrix} 0 & 1 & 0 & 0 \\ -\omega_1{}^2 & -2\gamma_1\,\omega_1 & -R1 & 0 \\ 0 & 0 & 0 & 0 \\ 0 & 0 & 0 & 0 \end{bmatrix} \begin{bmatrix} \eta \\ \dot{\eta} \\ V_p \\ V_s \end{bmatrix} + \begin{bmatrix} 0 & 0 & 0 \\ Q_1 & 0 & 0 \\ 0 & \frac{1}{C_p} & 0 \\ 0 & 0 & \frac{1}{C_s} \end{bmatrix} \begin{bmatrix} e^{i\omega t} \\ i_p \\ s \end{bmatrix} \tag{3.67}$$

The model used as basis for this work is based on the Erturk and Inman theory, and is implemented in matlab-simulink simulation software in order to be applied to some case studies detailed in chapter 4.

CHAPTER 4

Case study simulation

4 Case study simulation

4.1 Introduction

In this chapter the experimental study of piezoelectric sensors is addressed using MATLAB Simulink® software for the harvester system simulation. The obtained simulation results are verified using the EFM32 Giant Gecko Starter Kit.

For the modelling the MATLAB Simulink® version R2015a, CPU intel core i5 and Dormand - Prince iteration method are used.

4.2 Modelling piezoelectric energy harvesting system using MATLAB Simulink®

In the performed simulation a QP20W piezo film is used as a basic vibration energy harvesting sensor. As previously referred, the vibration energy harvesting system consist of two parts, the mechanical and electrical part, where the mechanical part used to simulate the sensor input.

In this work the considered input is vibration and the piezo sensor is working without load, i.e, in open circuit, as shown in Figure 4.1.

The mechanical part is constituted by: Signal Builder, which is used to implement rectangular signal with 0.2 second duration and 1 Newton of amplitude; Simulink-PS Converter Converts the unit less Simulink input signal into a physical signal; Ideal Force Source represents an ideal source of force that generates force proportional to the input physical signal; Mechanical Translational Reference, represents a mechanical translational reference point; Ideal Translational Motion Sensor converts an across variable measured between two mechanical translational nodes into a control signal proportional to velocity and position; Piezo Stack represent the piezoelectric sensor; Translational Damper represents an ideal mechanical translational viscous damper with 12 N(m/s) and the Translational Spring is an ideal mechanical linear spring with 10 N/m value.

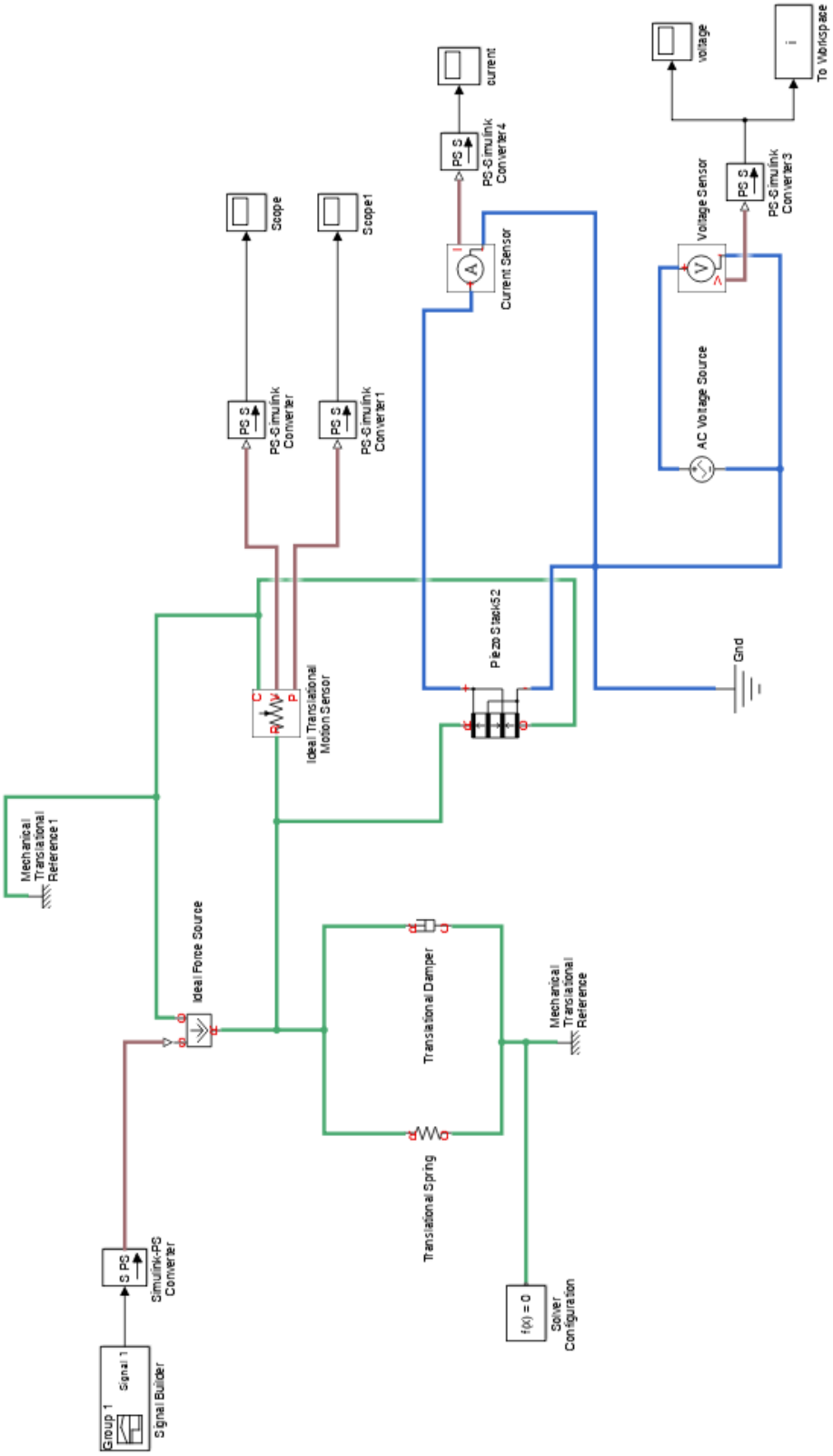

Figure 4.1 - Basic MATLAB Simulink® model of QP20W piezo film

The Piezo Stack represent the piezoelectric sensor QP20W which parameters are shown in figure 4.2.

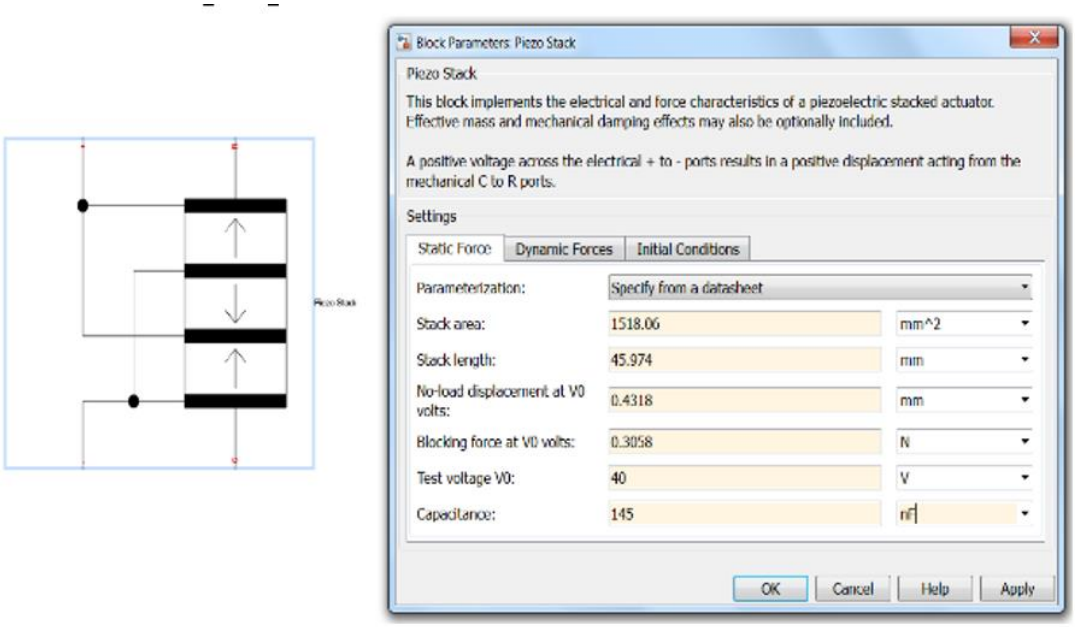

Figure 4.2 - QP20W piezo film parameters

The simulation result of piezoelectric sensor output voltage when a force of 1 Newton is applied is shown in figure 4.3.

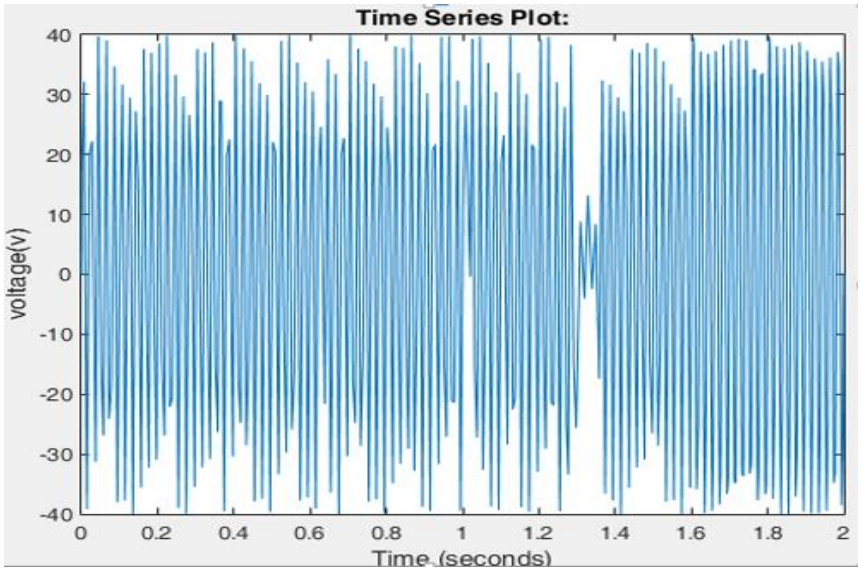

Figure 4.3 – Output voltage of Basic MATLAB Simulink® model of QP20W piezo film

4.3 Experimental Validation of the Piezo system Simulink® model

Using differential oscilloscope commonly characterized with high input resistance, the results from Simulink model are verified, where the output voltage of the piezo film laboratorial test is shown in figure 4.4.

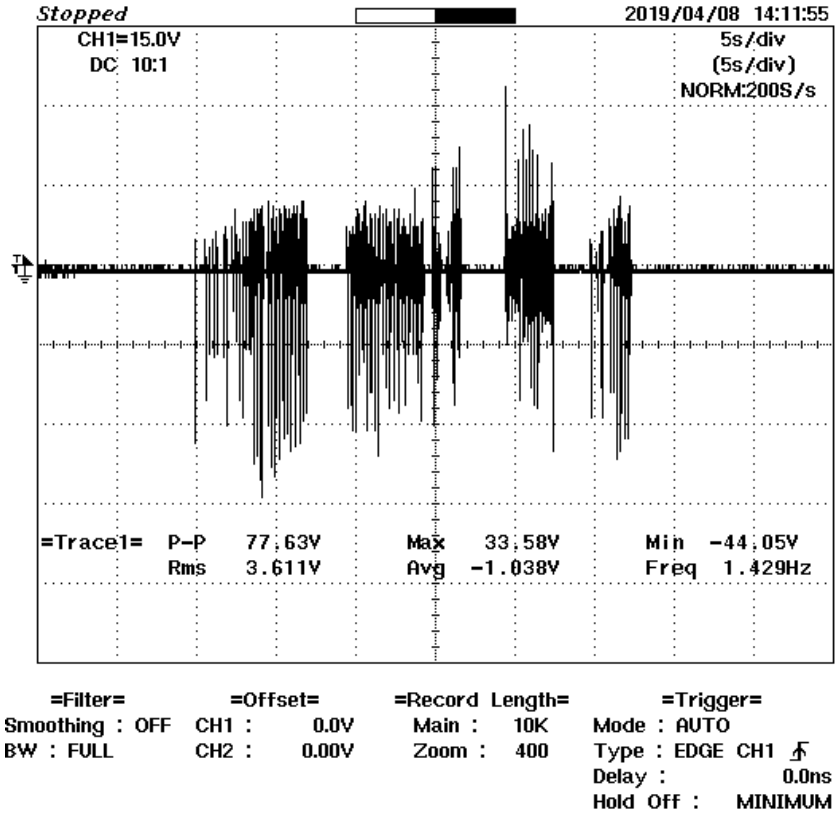

Figure 4.4 – Output voltage of laboratory test QP20W piezo film

In order to obtain output voltage signal, some pressure is applied on the piezoelectric sensor. This practical test is made just pressuring and alleviating that pressure with some frequency, in order to produce a mechanical vibration. Because this procedure is human performed is hard to produce always the same pressure with a constant frequency. Nevertheless, this simple test, allowed to observe and compare the voltage maximum amplitude value, with the results obtained in simulation. The total produced energy validation is more demanding and requires constant pressure and frequency applied on the sensor. Considering a simple

validation approach to the output voltage amplitude maximum is possible to observe an error that don´t exceed 5%.

4.4 Piezoelectric energy harvesting system simulation connected to a capacitor

Considering the addition of a capacitor in the system for energy storage and also an electrical load characterized by a resistor, the resulting matlab-simulink model is shown in Figure 4.5.

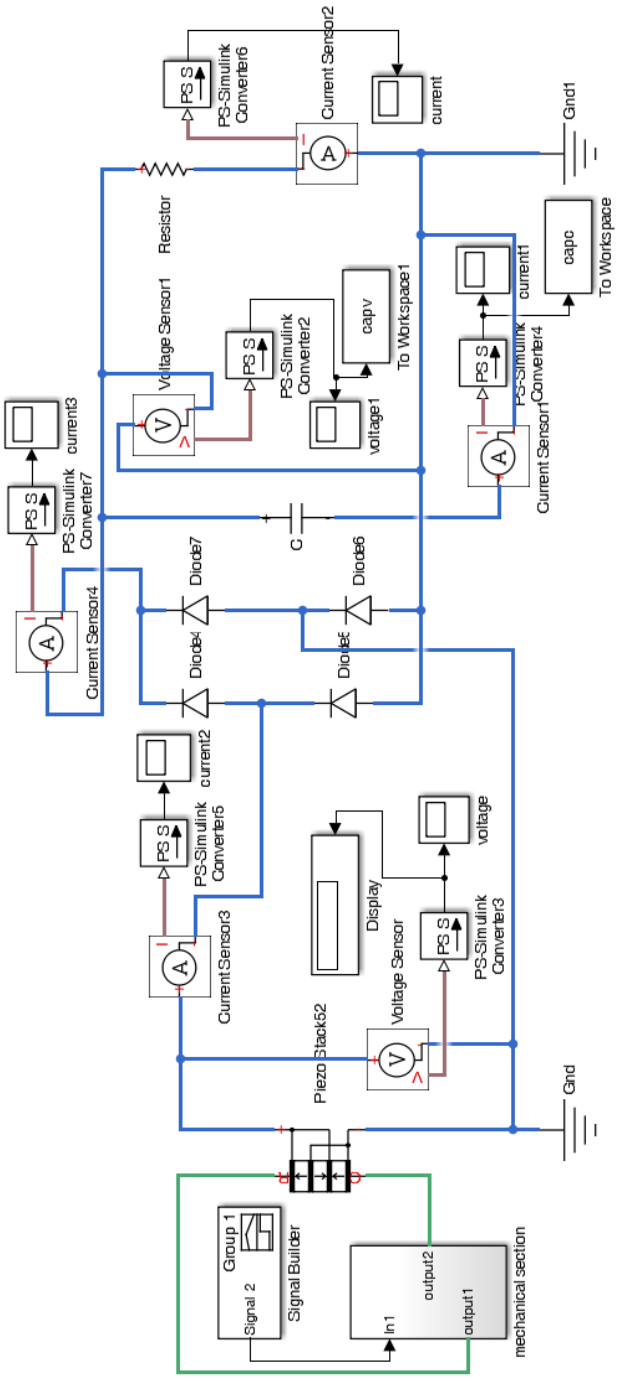

Figure 4.5 - Basic MATLAB Simulink® model of QP20W piezo connected to a storage capacitor

This system allows the storage of the small energy generated the piezoelectric vibrational energy harvester.

In this simulation 1000 μF capacitor is used and 1000 kΩ resistor is used as load. The diode bridge for full wave rectification is used to convert the output of the piezoelectric sensor from AC to DC in order to be applied into the capacitor (or even in a battery).

In Figure 4.6 the detailed the mechanical part of simulation model.

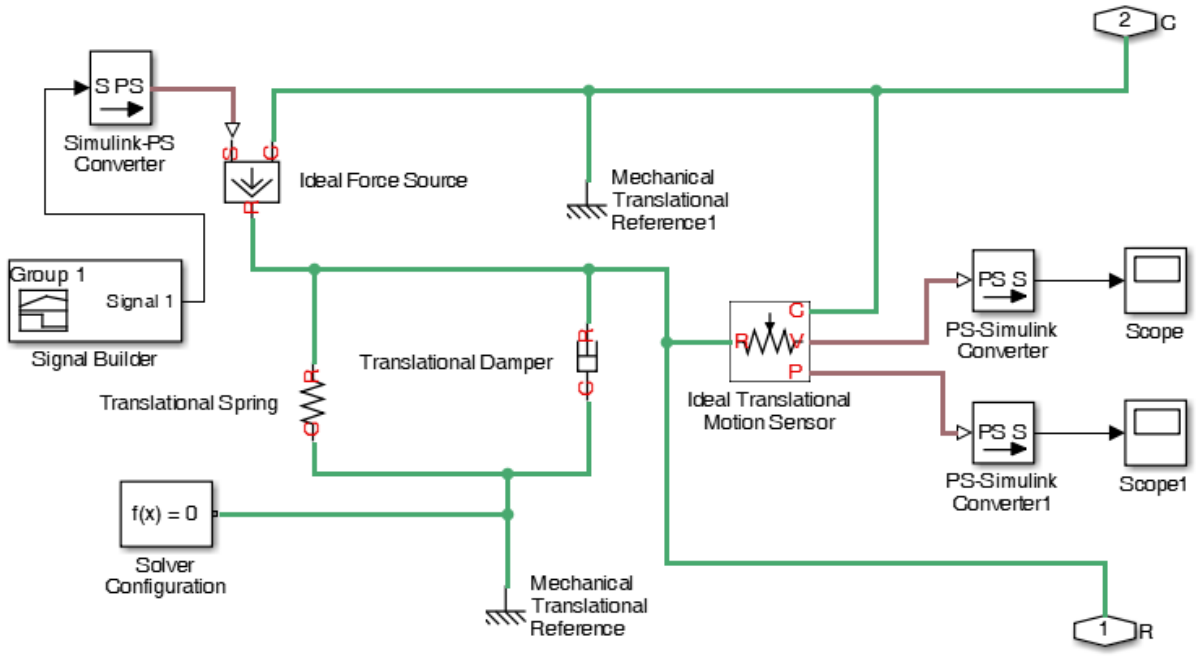

Figure 4.6 - Mechanical part of MATLAB Simulink® model of QP20W piezo film

The simulation result of voltage and the current through the storage capacitor are shown in Figure 4.7 and Figure 4.8, respectively.

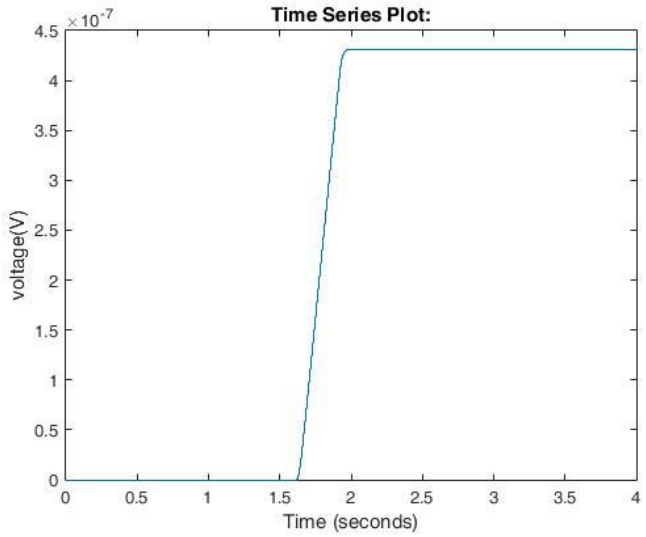

Figure 4.7 - Voltage through storage capacitor

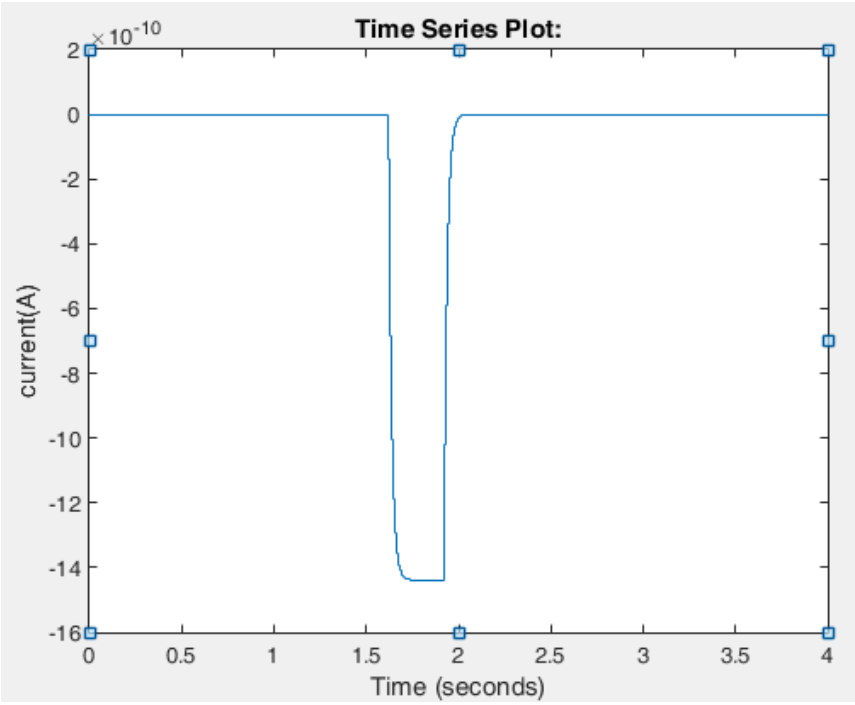

Figure 4.8 - Current through the storage capacitor simulated using MATLAB Simulink®

The values shown in Figures 4.7 and 4.8 are almost insignificant. However, is important to highlight that this simulation is performed considering a single piezo film sensor. A scale factor is not considered because just one piezo film sensor is physically available for the system validation. The validation is performed using a commercial kit described in chapter 4.5.

The capacitor energy storage can be obtained accordingly with (4.1).

$$E_{cap} = \frac{CV^2}{2} \tag{4.1}$$

Where E_{cap} is the capacitor energy, C is the capacitance and V the voltage. Considering in this case study 1000 μF, 42.5 μV, results on an stored energy of 9.03×10^{-7} J.

4.5 Validation of Piezo system model connected to a storage capacitor

In order to accomplish some validation data, EFM32 Giant Gecko Starter Kit and Simplicity Studio® software are used. In figure 4.9 is shown the output from the used kit that, in this work, is considered as reference for comparison with simulation results from matlab-simulink.

Figure 4.9 - Current through the storage capacitor simulated using EFM32 Giant Gecko Starter Kit and Simplicity Studio® software

In figure 4.8 a positive spike signal is present even without connecting any input to the kit. It can be inferred that these positive spike signal may cause by the discharge of some capacitors present in the kit used to perform physical tests. It also can be observed that the current in the storage capacitor is near 1 nA, against the 1.4 nA observed in figure 4.9. Figure 4.10 results from a zoom applied to the area where capacitor current is registered.

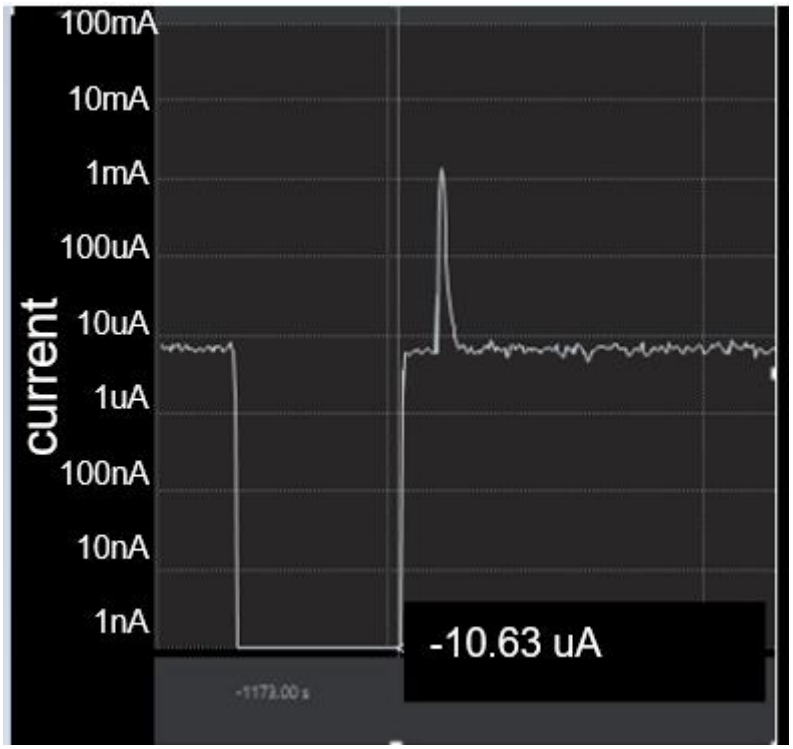

Figure 4.10 – Current zoom through the storage capacitor simulated using EFM32 Giant Gecko Starter Kit and Simplicity Studio® software

In figure 4.10 is possible to observe a time frame of approximately 5 ms that is in line of the approximately 4 ms observed in figure 4.8.

4.6 Macro-scaled of piezoelectric energy harvester

In order to analyse a macro-scaled application of piezoelectric energy harvester in a simulation context, a set of 60 QP20W piezo film units is considered. This set is constituted by 2 parallel subsets of 30 unit sensors connected in series.

A simulink model of a macro-scale implementation is shown in figure 4.11.

Considering this macro-scale approach a simulation result of voltage and the current through the storage capacitor are shown in Figure 4.12 and Figure 4.13, respectively.

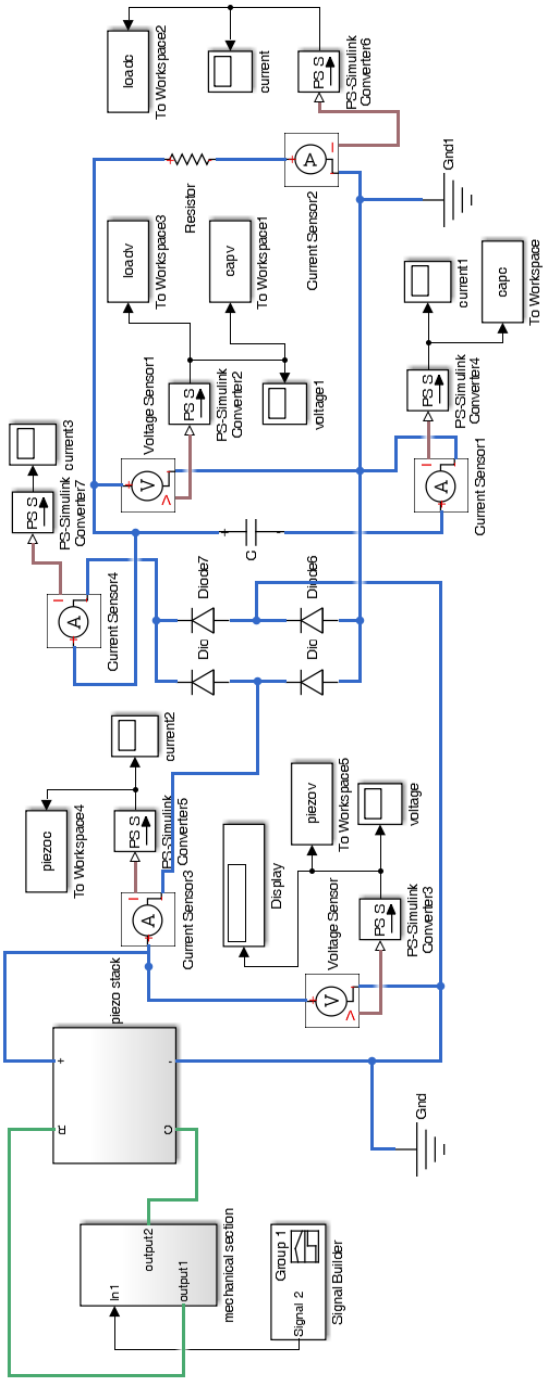

Figure 4.11- Macro-scaled of piezoelectric energy harvester

It can be observed that when sensor are clustered into sets, is possible to increase the output voltage. In this case, the voltage increased from approximately 0.43mV to near 18V, which allows some applications into small electric devices.

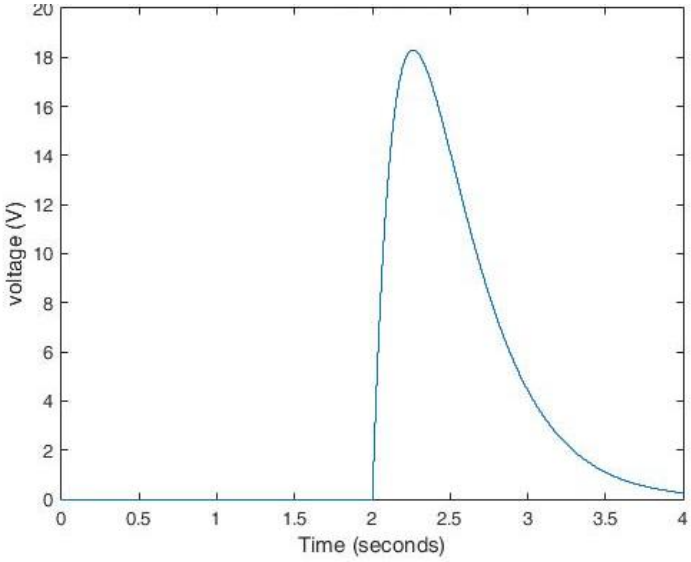

Figure 4.12 –Output voltage from a set of 60 piezo film sensors

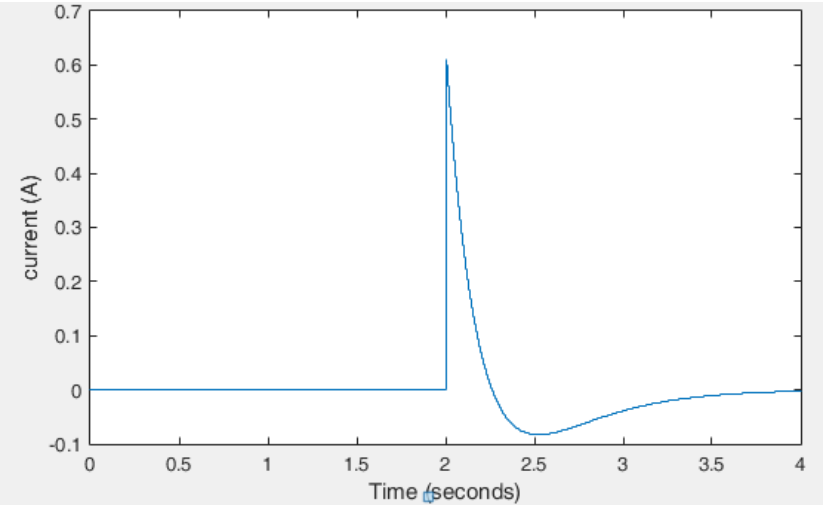

Figure 4.13 - Current in a set of 60 piezo film sensors

As result of using a set of 60 piezo sensors, the output voltage increased to 18 V as shown in Fig. 4.12, resulting in a current applied to the load given in Figure 4.14.

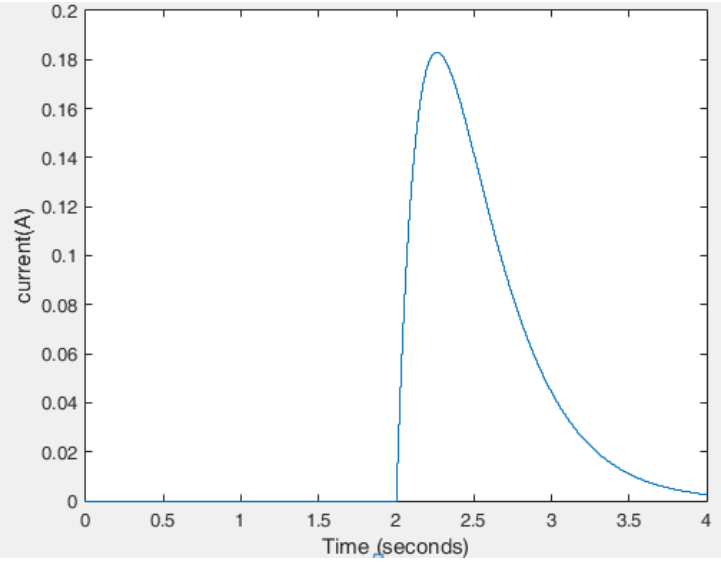

Figure 4.14 - Current through the load resistor simulated using MATLAB Simulink®

4.7 Application development of piezoelectric vibration sensor

A simple practical experiment shown in figure 4.15, is implemented where a QP20W piezo film sensor is applied to an electrical load, represented by a led. So, when the piezo sensor vibrates or is pressed the circuit starts working, turning the led light on.

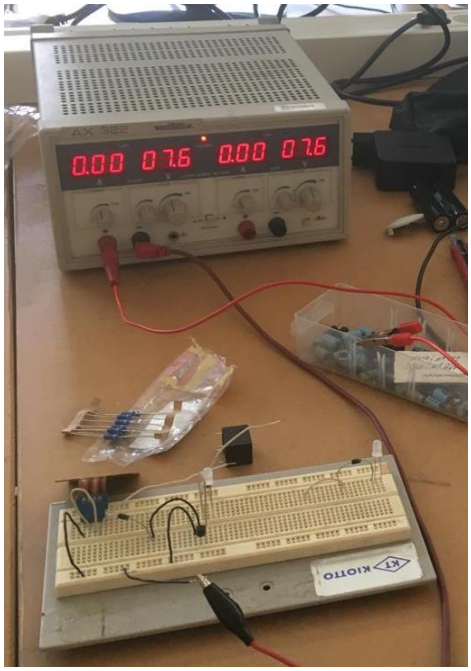

Figure 4.15 - Experimental design piezo film applied to a led

An on-off vibration switch represented in figure 4.16 is applied on a QP20W piezo sensor.

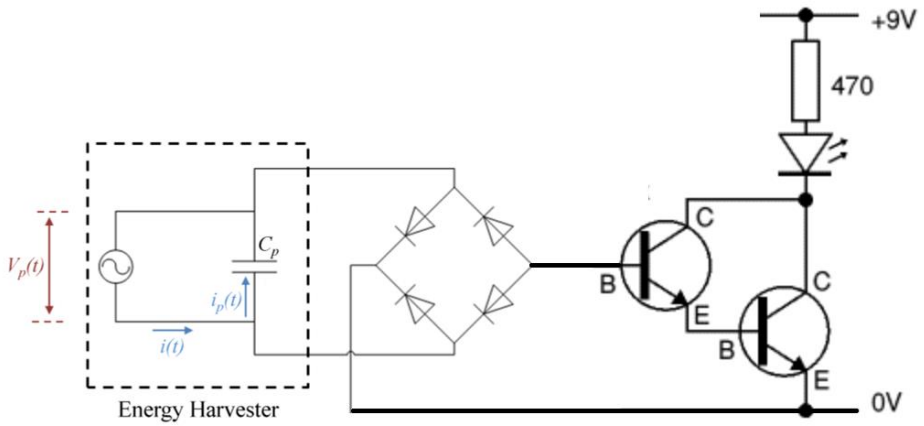

Figure 4.16 – Electric schematic diagram of on-off switch

The electric circuit consists on a Darlington amplifier using 2 NPN transistors. The design structure is accomplished by two transistors connected in such a way that the current amplified by the first transistor is further amplified by the second one, so this connection provides a higher current gain. A full bridge rectifier is used to convert the output of the piezoelectric sensor from AC to DC and the led light is used to indicate to the output.

A full bridge rectifier used to convert the output of the piezoelectric sensor from AC to DC, because the NPN transistor needs a DC voltage (minimum 0.7V) as a trigger signal (input signal) to be apply in the base in order to change the situation of the collector emitter connection (turning on the output) as it shown in Figure 4.17.

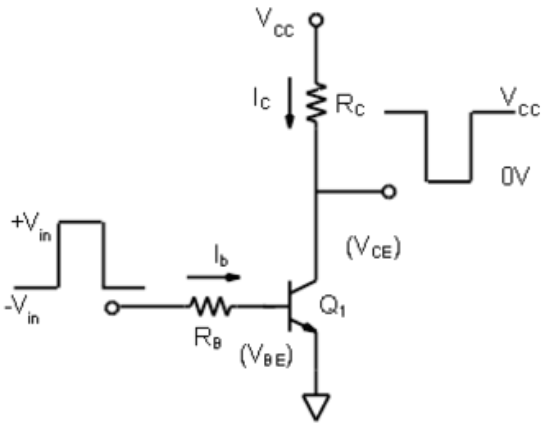

Figure 4.17 – Electrical scheme of the NPN transistor

CHAPTER 5

Conclusions

5 Conclusions

In this work a study and analysis of a rectangular cantilever piezoelectric energy harvesters system is detailed. The harvesting sources some existing and piezoelectric sensors were identified and detailed, supporting the choice of a vibration energy source applied to a structure piezo film considered in the present developed work.

Several mathematical models were analysed and the developed work is based on the three mathematical models addressed in chapter 3. These models are used to emulate the piezoelectric film functioning and calculate the predicted output. Those three kind of mathematical models complement each other, in way that increase model complexity in order to include the significant physical characteristics, namely, the vibroimpacting electromechanical effects, direct and inverse effect and energy dissipation

A MATLAB Simulink® model based on previous mention mathematical model was implemented in order to simulate the QP20W piezo film sensor. The simulation results showed an expected generated output, in line with de validation experimental tests performed, as shown in chapter 4. This validation experimental test was accomplished using a differential oscilloscope, characterized by a high electrical internal resistance, giving the maximum voltage output of the piezo sensor with and error inferior to 5%.

A capacitor was included in the implemented simulation model allowing to study the system performance including energy storage. In this system an electrical load, represented by a resistor is considered and the voltage and current outputs obtained are detailed in chapter 4. This simulation model was also validated using the EFM32 Giant Gecko Starter Kit and Simplicity Studio® software, resulting on an observed error of approximately 8%.

Regarding the importance to enhance the obtained energy harvesting, turning possible its usage in various applications, a macro-scale of piezoelectric energy harvester was considered, including a set of 60 QP20W piezo film used to build a Macro-scale of piezoelectric energy harvester system. A darlington circuit, full bridge rectifier, led light and QP20W piezo sensor

were used to build an on-off switch vibration, and in this design a led light was used to indicate to the output. So, it was verified that when the piezo sensor is vibrating or even pressed led light turns on.

From this study is possible to infer that the piezoelectric harvesting energy is able to provide a relevant energy source that is otherwise neglected and unused. However is important to highlight that there as other harvesting sources, no less important than vibration energy source, as solar energy, for instance.

If a set of piezoelectric sensor are implemented in one panel and installed in the highways it is possible to start generating energy when the cars are passing over these panels, or even if several piezoelectric panel were installed on the both highway sides taking advantage on the vibration caused by wind generated from cars movement. In addition, other vibration energy source could be any noisy place.

References

[1] P. Dineva et al., Dynamic Fracture of Piezoelectric Materials, 7 Solid Mechanics and Its Applications 212, DOI: 10.1007/978-3-319-03961-9_2, © Springer International Publishing Switzerland 2014

[2] Energy Generation by using PIEZOELECTRIC MATERIALS and Its Applications https://www.slideshare.net/AnimeshSachan/my-seminar-46313881

[3] DOCTORAT DE LUNIVERSITÉ DE TOULOUSE Délivré par : Institut National Polytechnique de Toulouse (INP Toulouse) Discipline ou spécialité : Génie Électrique

[4] K. H. Mak, Vibration Modelling and Analysis of Piezoelectric Energy Harvesters, Ph.D. thesis, University of Nottingham, University Park, Nottingham, UK, 2011.

[5] Lippmann, G. Principe de la conservation de l'électricité (http://gallica.bnf.fr/ark:/12148/bpt6k348640) [Principle of the conservation of electricity]. Annales de chimie et de physique (in French). 24: 145. Archived from the original on 2016-02-08.

[6] Curie, Jacques; Curie, Pierre (1881). Contractions et dilatations produites par des tensions dans les cristaux hémièdres à faces inclines (https://web.archive.org/web/20121205084840/http://gallica.bnf.fr/ark:/12148/bpt6k3049g/f1131.image) from the original on 2012-1205.

[7] Voigt, Woldemar Lehrbuch der Kristallphysik (1910).

(https://books.google.com/books?id=SvPPAAAAMAAJ&pg=PR1#v= onepage&q&f=false). Berlin: B. G. Teubner. (https://web.archive.org/web/20140421051401/http://books.google.

com/books?id=SvPPAAAAMAAJ&pg=PR1#v=onepage&q&f=false) from the original on 2014-0421.

[8] https://www.sintef.no/projectweb/piezomems/about-piezomems/

[9] (https://ec.europa.eu/programmes/horizon2020) Published on Horizon 2020

[10] C. J. Chen, Physics of Solar Energy, Hoboken, New Jersey: John Wiley & Sons, Ltd, 2011.

[11] S. Beeby and N. White, Energy Harvesting For Autonomous Systems, Norwood, Massachusetts: Artech House, 2010.

[12] S. Priya and D. J. Inman, Energy Harvesting Technologies, New York, USA: Springer Science + Business Media, 2009.

[13] S. Roundy, P. K. Wright and J. Rabaey, A study of low level vibrations as a power source for wireless sensor nodes, Journal of Computer Communication, 26, pp. 1131–1144, 2003.

[14] V. Raghunathan, A. Kansal, J. Hsu, J. Friedman and M. Srivastava, Design Considerations for Solar Energy Harvesting WIreless Embedded Systems,Fourth IEEE/ACM International Conference on Information Processing in Sensor Networks, 2005.

[15] E. Dawidowicz,Wind Energy Harvesting for Low Power Applications,SAE International Journal of Aerospace, vol. 1, no. 1, pp. 883-886, 2009.

[16] R. Ang, Y. Tan and S. Panda, Energy Harvesting for Autonomous Wind Sensor in Remote Area,33rd Annual Conference of IEEE Industrial Electronics Society, pp. 2104-2109, 2007.

[17] E. Carlson, K. Strunz and B. Otis, A 20mV Input Boost Converter with Efficient Digital Control for Thermoelectric Energy Harvesting, IEEE Journal of SolidState Circuits, vol. 45, no. 4, pp. 741-750, 2010. 74

[18] M. Koplow, A. Chen, D. Steingart, P. Wright and J. Evans, Thick Film Thermoelectric Energy Harvesting Systems for Biomedical Applications, IEEE 5th International Summer School and Symposium on Medical Devices and Biosensors, pp. 322-325, 2008.

[19] J. G. Smits: The constituent equations of piezoelectric heterogeneous bimorphs. Proceedings of IEEE Ultrasonics Symposium, vol. 3, 1990, pp. 1275 - 1278

[20] piezo film product guide and price list , MEASUREMENT SPECIALTIES, INC. www.meas-spec.com

[21] Design and simulation of piezoelectric energy harvesting system , M.Bhanusri, Department of physics, IIT MADRAS , comsol conference Bangalore 2013

[22]. V. Ostasevicus, R. Dauksevicius, Microsystem Dynamics, Springer, 2010.

[23]. IEEE Ultrasonics, Ferroelectrics, and Frequency Control Society, - IEEE Standard on Piezoelectricity, 176-1987,1988.

[24] MECH 466 Microelectromechanical Systems,University of Victoria Dept. of Mechanical Engineering, Lecture 11: Piezoelectric Sensors & Actuators

[25] R. W. Clough and J. Penzien, Dynamics of Structures, United States of America: McGraw-Hill, 1975

[26] A. Erturk and D. J. Inman, A distribution parameter electromechanical model for cantilever piezoelectric energy harvesters, Journal of Sound and Acoustics, 130, p. 041002 (15 pp), 2008.

[27] K. B. Oldham and J. Spanier, The Fractional Calculus, New York, America: Academic Press, 1974.

[28] F. S. Tse, I. E. Morse and H. R. T., Mechanical Vibration Theory and Applications - Second Edition, Boston, Massachusetts: Allyn and Bacon, 1978.

[29] W. J. Weaver, S. P. Timoshenko and D. H. Young, Vibration Problems In Engineering, Canada: John Wiley & Sons, Ltd, 1990.

[30] IEVA MILAŠAUSKAITĖ RESEARCH OF DYNAMICS OF PIEZOELECTRIC ENERGY HARVESTERS Doctoral Dissertation Technological Sciences, Mechanical Engineering (09T)

[31] Meijering, Erik A chronology of interpolation: from ancient astronomy to modern signal and image processing (PDF). Proceedings of the IEEE. 90 (3): 319–342. doi:10.1109/5.993400, (2002).

[32] https://www.sciencedirect.com/topics/engineering/kelvin-voigt-model

[33] Comparison of Modal Parameters Extracted Using MIMO, SIMO, and Impact Hammer Tests on a Three-Bladed Wind Turbine, Experimental Mechanics Series 2014, pp 185-197

[34] MIDE , quick pack PACKAGED PIEZOELECTRIC ACTUATORS AND SENSORS QP20W .

APPENDIX

DESCRIPTION

Energy Harvesting (EH)

Multi-Source Demo Board with Transducers

The DC2080 is a versatile energy harvesting demo board that is capable of accepting piezoelectric, solar, 4mA to 20mA loops, thermal powered energy sources or any high impedance AC or DC source. The board contains four independent circuits consisting of the following EH ICs:

- LTC®3588-1: Piezoelectric Energy Harvesting Power Supply
- LTC3108: Ultralow Voltage Step-Up Converter and Power Manager
- LTC3105: Step-Up DC/DC Converter with Power Point Control and LDO Regulator
- LTC3459: 10V Micropower Synchronous Boost Converter
- LTC2935-2 and LTC2935-4: Ultralow Power Supervisor with Power-Fail Output Selectable Thresholds

The board is designed to connect to the Energy Micro STK development kit. It also includes two energy harvester

QUICK START PROCEDURE

BOARD PHOTO

transducers (TEG and Solar) and a terminal block for connecting a high impedance AC source. In addition, many turrets are provided, making it easy to connect additional transducers to the board.

The board contains multiple jumpers that allow the board to be configured in various ways. The standard build for the board has 4 jumpers installed out of the possible 12 jumpers. The board is very customizable to the end users' needs. This compatibility makes it a perfect evaluation tool for any low power energy harvesting system.

Please refer to the individual data sheets for the operation of each power management circuit. The application section of this demo manual describes the system level functionality of this board and the various ways it can be used in early design prototyping.

Design files for this circuit board are available.

Refer to Figures 2, 3 and 4 for the proper equipment setup and jumper settings for the following quick start procedure.

1. Configure the equipment and jumpers as shown in Figure 2. Verify the jumper settings are as follows:
   - JP1 OPEN
   - JP2 OPEN
   - JP3 OPEN
   - JP4 OPEN
   - JP5 OPEN
   - JP6 OPEN
   - JP7 OPEN
   - JP8 **OPEN**
   - JP9 **INSTALLED in "ON" Position**
   - JP10 OPEN
   - JP11 OPEN
   - JP12 **INSTALLED**
2. Slowly increase PS1 and observe the voltage at which VM2 turns on. VM1 should be equal to approximately 3.15V.
3. Slowly decrease PS1 towards zero. Observe the voltage on VM1 at which VM2 drops rapidly to 0V. VM1 should be equal to approximately 2.25V.
4. Turn off PS1 and remove all test equipment.
5. **Install JP4** and connect the Energy Micro starter kit board to J1.
6. Apply a light source and observe the starter kit turning on and displaying the temperature of the microcontroller.
7. **MOVE JP4 to JP2** and place a warm object, such as your hand, firmly on the entire TEG1, thermal electric generator.
8. Observe the starter kit turning on and displaying the temperature of the microcontroller.
9. **MOVE JP4 to JP1**. Disconnect the Energy Micro starter kit from J1.
10. Set PS2 equal to 6.0V. Reconfigure the test equipment as shown in Figure 3.
11. Turn on PS2. Observe the voltage on VM1 and VM2. The voltage on VM1 should be approximately 5.77 Volts and on VM2 should be 3.3V.
12. Use VM3 to observe the voltage on JP5-2. The voltage should be equal to the same level observed on VM2.
13. Turn off PS2
14. **MOVE JP1 to JP3.** Disconnect PS2 from the board and set PS3 equal to 5.0V. Reconfigure the test equipment as shown in Figure 4.
15. Turn on PS3. Observe the voltage on VM1 and VM2. The voltage on VM1 should be approximately 0.34 Volts and on VM2 should be 3.3V.

Figure 1. DC2080A Connected to an Energy Micro Starter Kit in the "To Go" Design Kit for Energy Harvesting

QUICK START PROCEDURE

16. Use VM3 to observe the voltage on JP7-2. The voltage should be approximately equal to the level observed on VM2.
17. Turn off PS3
18. Reset the Jumpers as shown in Figure 5a.

JP1 OPEN

JP2 OPEN

JP3 OPEN

JP4 **INSTALLED**

JP5 OPEN

JP6 OPEN

JP7 OPEN

JP8 **OPEN**

JP9 **INSTALLED in "ON" Position**

JP10 OPEN

JP11 **INSTALLED**

JP12 OPEN

QUICK START PROCEDURE

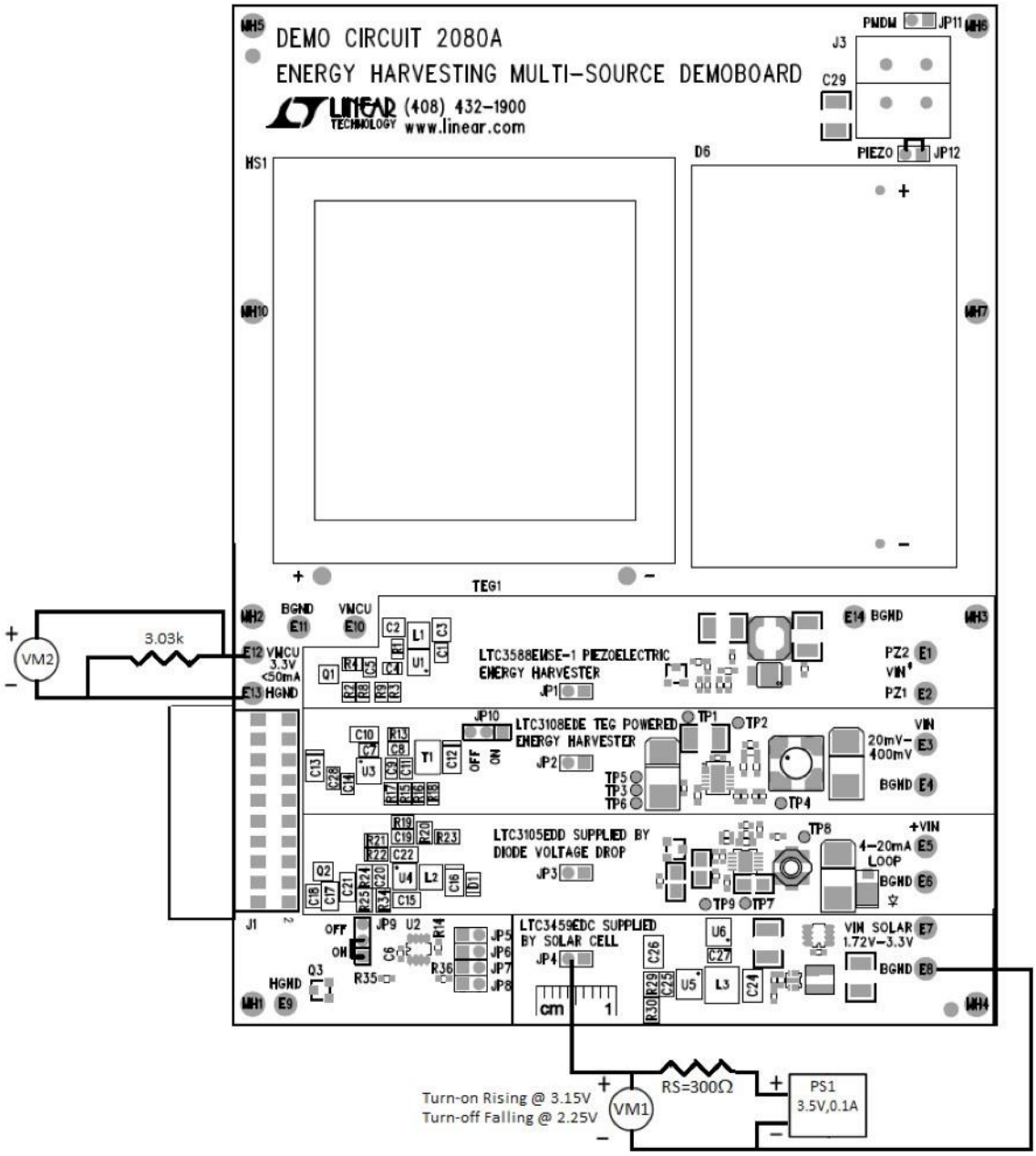

Figure 2. VMCU Power Switchover Test Setup

QUICK START PROCEDURE

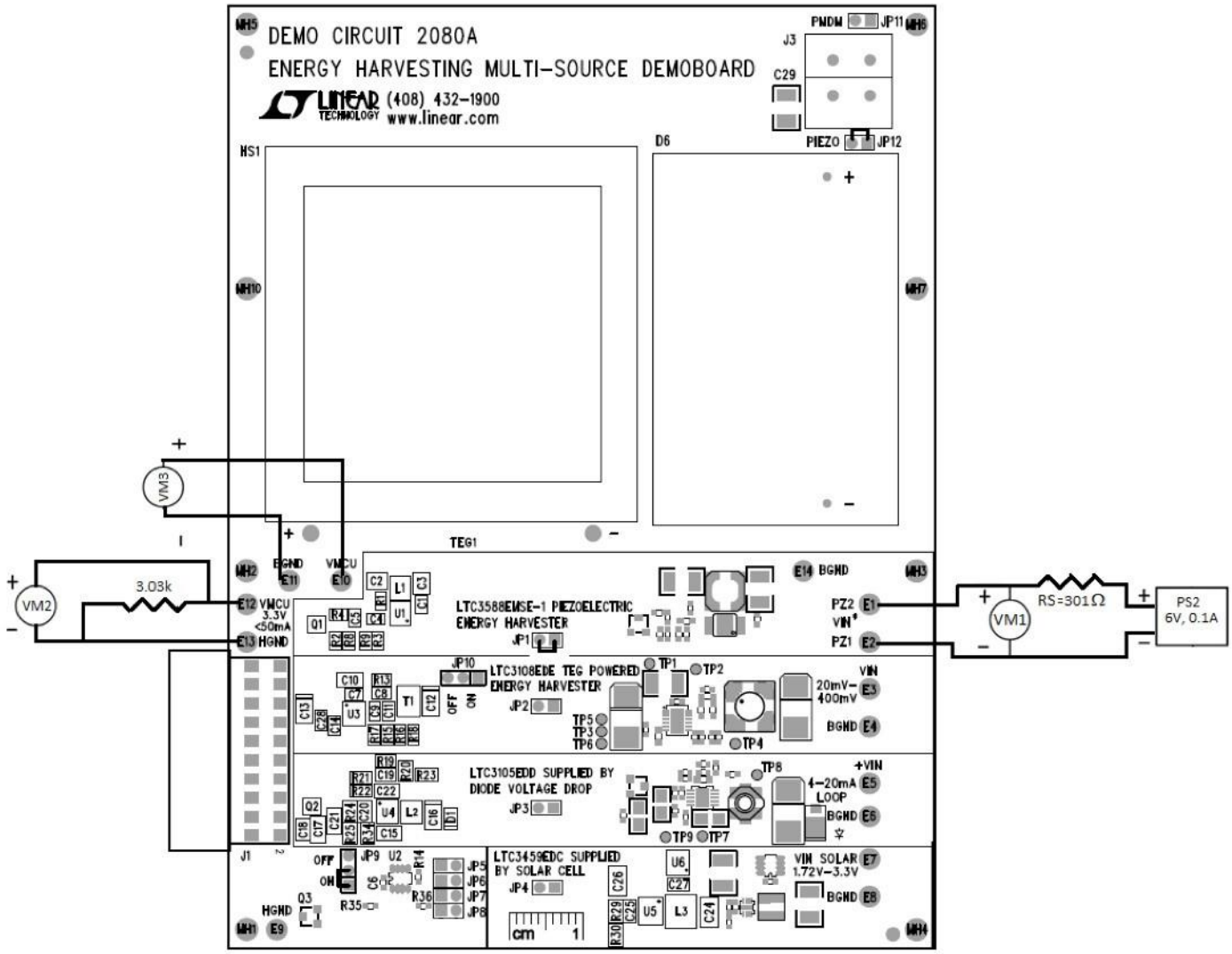

Figure 3. Piezoelectric Circuitry Test Setup. Proper Measurement Equipment Setup for DC2080A Piezoelectric Circuit Testing

QUICK START PROCEDURE

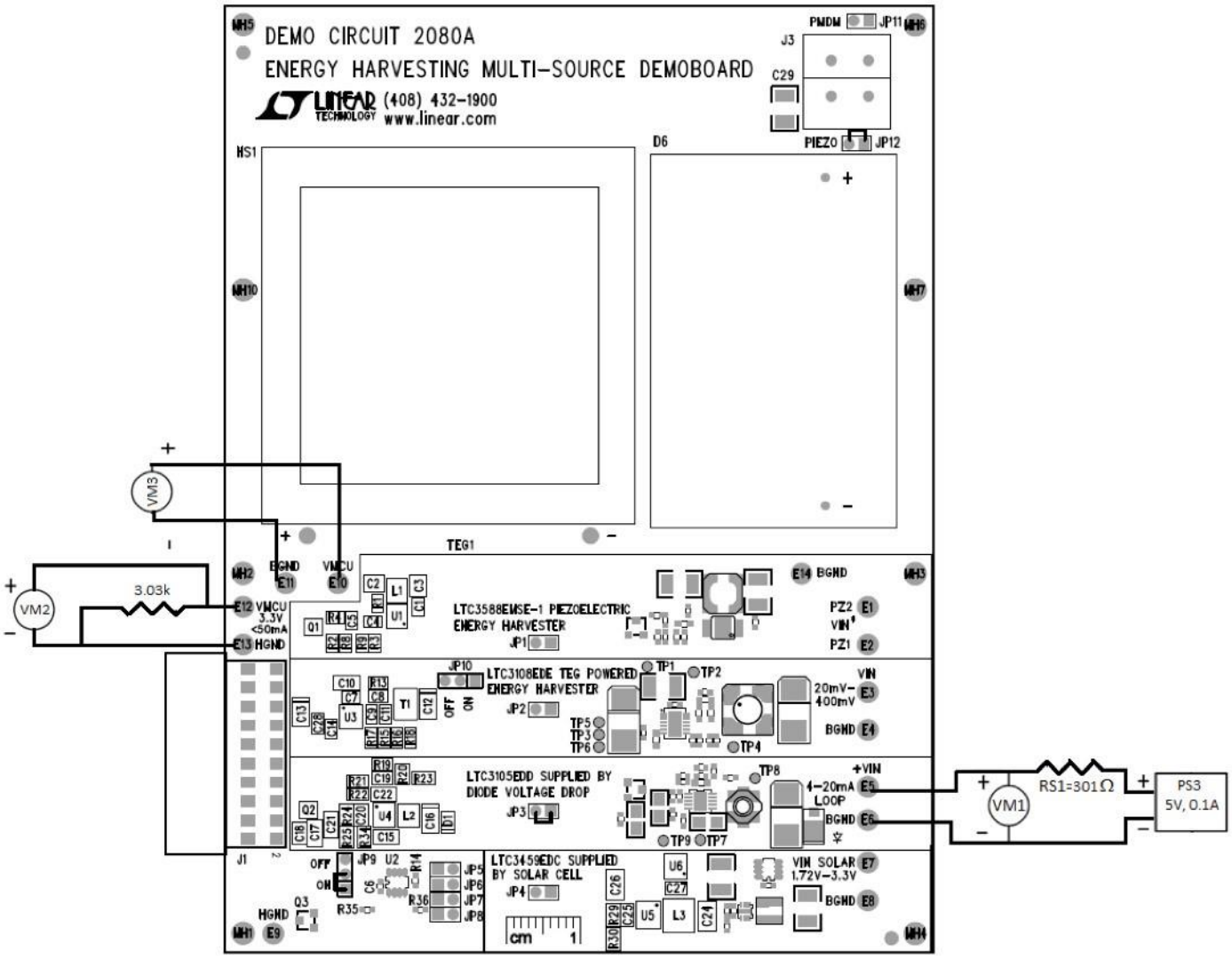

Figure 4. 4mA to 20mA Loop Circuitry Test Setup. Proper Measurement Equipment Setup for DC2080A 4mA to 20mA Loop Circuit Testing

QUICK START PROCEDURE

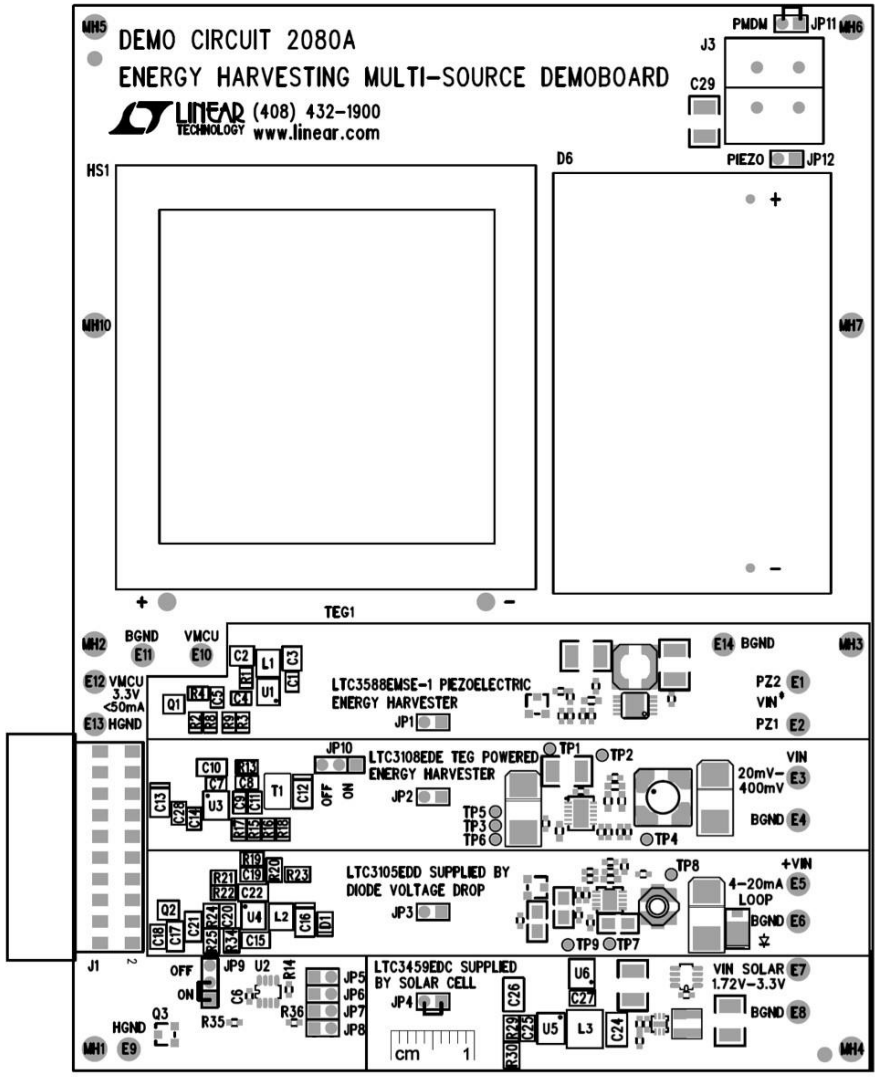

Figure 5a. DC2080A Top Assembly Drawing

QUICK START PROCEDURE

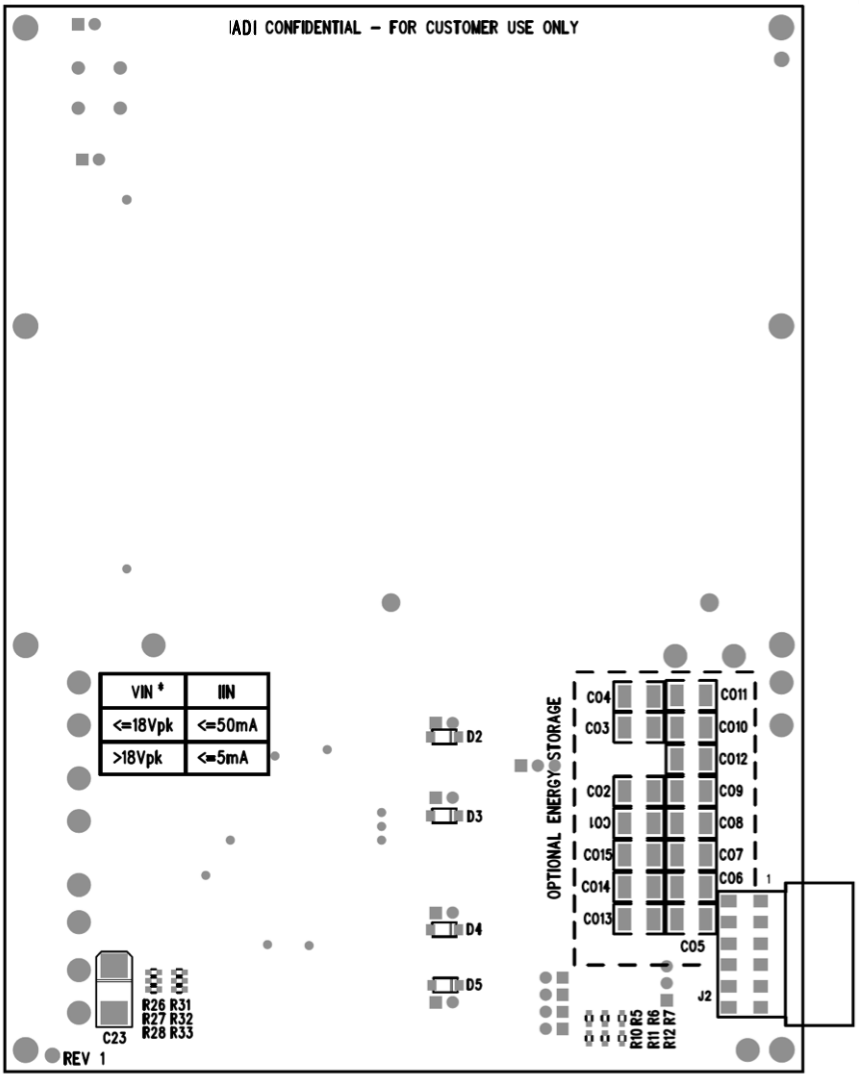

Figure 5b. DC2080A Bottom Assembly Drawing

APPLICATION

Jumper Functions

JP1: Power selection jumper used to select the LTC3588-1, Piezoelectric Energy Harvesting Power Supply.

JP2: Power selection jumper used to select the LTC3108, TEG Powered Energy Harvester.

JP3: Power selection jumper used to select the LTC3105, powered by a diode voltage drop in a 4mA to 20mA loop.

JP4: Power selection jumper used to select the LTC3459, powered by a solar panel.

JP5: Routes the LTC3588-1 PGOOD signal to the Dust header PGOOD output. The LTC3588-1 PGOOD comparator produces a logic high referenced to V_{OUT} on the PGOOD pin the first time the converter reaches the sleep threshold of the programmed V_{OUT}, signaling that the output is in regulation. The PGOOD pin will remain high until V_{OUT} falls to 92% of the desired regulation voltage. Additionally, if PGOOD is high and V_{IN} falls below the UVLO falling threshold, PGOOD will remain high until V_{OUT} falls to 92% of the desired regulation point. This allows output energy to be used even if the input is lost.

JP6: Routes the LTC3108 PGOOD signal to the header PGOOD output.

JP7: Routes the LTC3105 PGOOD signal to the header PGOOD output.

JP8: Routes the LTC3459 PGOOD signal to the header PGOOD output.

JP9: Connects the fifteen optional energy storage capacitors directly to V_{OUT} to be used by the load to store energy at the output voltage level. The 100µF capacitors have a voltage coefficient of 0.61 of their labeled value at 3.3V and 0.47V at 5.25V. **CAUTION: Only JP9 OR JP10 may be connected at any one time. Do not populate both JP9 and JP10.**

JP10: Connects the fifteen optional energy storage capacitors directly to VSTORE of the LTC3108 TEG powered energy harvester circuit, which is the output for the storage capacitor or battery. A large capacitor may be connected from VSTORE to GND for powering the system in the event the input voltage is lost. It will be charged up to the maximum VAUX clamp voltage, typically 5.25 Volts. The 100µF capacitors have a voltage coefficient of 0.47V at 5.25V. **CAUTION: Only JP9 OR JP10 may be connected at any one time. Do not populate both JP9 and JP10.**

JP11: Configures the AC input for use with a PMDM vibration harvester, **CAUTION: Only JP11 OR JP12 may be connected at any one time. Do not populate both JP11 and JP12.**

JP12: Configures the AC input for use with any high impedance source including piezoelectric transducers, electromechanical transducers or AC mains supplies with high series resistance. C**AUTION: Only JP11 OR JP12 may be connected at any one time. Do not populate both JP11 and JP12.**

Turret Functions

PZ1 (E1): Input connection for piezoelectric element or other AC source (used in conjunction with PZ2). A high impedance DC source may be applied between this pin and BGND to power the LTC3588-1 circuit. **CAUTION: The maximum current into this pin is 50mA. PZ2 (E2):** Input connection for piezoelectric element or other AC source (used in conjunction with PZ1). A high impedance

APPLICATION

DC source may be applied between this pin and BGND to power the LTC3588-1 circuit. **CAUTION: The maximum current into this pin is 50mA. VIN, 20mV to 400mV (E3):** Input to the LTC3108, TEG powered Energy Harvester. The input impedance of the LTC3108 power circuit is approximately 3Ω, so the source impedance of the TEG should be less than 10Ω to have good power transfer. TEG's with approximately 3Ω will have the best power transfer. The input voltage range is 20mV to 400mV.

BGND (E4,E6,E8,E11,E14): This is the board ground. BGND is connected to all the circuits on the board except the headers. BGND and HGND, the header ground are connected through Q3 when the VMCU voltage with respect to BGND reaches the rising RESET Threshold of U2 and disconnected when VMCU falls to the falling reset threshold. The board is configured from the factory to connect BGND and HGND when VMCU equals 3.15V and disconnect them when VMCU equals 2.25V.

+VIN, 4mA to 20mA LOOP (E5): Input to the LTC3105 supplied by a diode voltage drop. The current into this terminal must be limited to between 4mA and 20mA. The current into this turret flows through diode D1 to generate the diode voltage drop and into the LTC3105 power management circuit.

VIN SOLAR (E7): Input to the LTC3459, solar powered circuit with maximum power point control, provided by the LTC2935-4. The input regulation point for the MPPC function is 1.73V. The input range is 1.72V to 3.3V.

HGND (E9,E13): This is the header ground. HGND is the switched ground to the header that ensures the load is presented with a quickly rising voltage. BGND and HGND are connected through Q3 when the VMCU voltage with respect to BGND reaches the rising RESET Threshold of U2 and disconnected when VMCU falls to the falling reset threshold. The board is configured from the factory to connect BGND and HGND when VMCU equals 3.15V and disconnect them when VMCU equals 2.25 Volts.

VMCU (E10,E12): Regulated output of all the active energy harvester power management circuits, referenced to BGND. When VMCU is referenced to HGND it is a switched output that is passed through header, J1 to power the load.

LTC3588-1: Piezoelectric Energy Harvesting Power Supply (Vibration or High-Impedance AC Source)

The LTC3588-1 piezoelectric energy harvesting power supply is selected by installing the power selection jumper JP1. The PGOOD signal can be routed to the header by installing jumper JP5.

If the application requires a wide hysteresis window for the PGOOD signal, the board has the provision to use the independent PGOOD signal, shown in Figure 10, generated by the LTC2935-2 and available on JP8. This signal is labeled as the PGOOD signal for the LTC3459 circuit (PGOOD_LTC3459), because the LTC3459 does not have its own PGOOD output. The PGOOD_LTC3459 signal can be used in place of any of the PGOOD signals generated by the harvester circuits. The board is configured from the factory to use the PGOOD_LTC3459 signal as the PGOOD signal to switch from battery power to energy harvesting power.

The PGOOD_LTC3459 signal is always used to switch the output voltage on the header. Some loads do not like to see a slowly rising input voltage. Switch Q3 ensures that VMCU on the header is off until the energy harvested output voltage is high enough to power the load. The

APPLICATION

LTC2935-2 is configured to turn on Q3 at 3.15V and turn off Q3 at 2.25V. With this circuit, the load will see a fast voltage rise at startup and be able to utilize all the energy stored in the output capacitors between the 3.15V and 2.25V levels.

The optional components R1, R4, Q1 and C5 shown on the schematic are not populated for a standard assembly. The function of R1, R4, Q1 and C5 is to generate a short PGOOD pulse that will indicate when the output capacitor is charged to its maximum value. The short pulse occurs every time the output capacitor charges up to the output sleep threshold, which for a 3.3V output is 3.312V. By populating these components the application can use this short pulse as a sequence timer to step through the program sequence or as an indication of when it can perform energy-intensive functions, such as a sensor read or a wireless transmission and/or receive, knowing precisely how much charge is available in the output capacitors. When this optional circuit is not used, the amount of charge in the output capacitors is anywhere between the maximum (C_{OUT} • V_{OUT_SLEEP}) to eight percent low. In the case where the energy harvesting source can support the average load continuously, this optional circuit is not needed.

Diode D2 is an optional component used to diode-OR multiple energy harvesting sources together. This diode would be used in conjunction with one or more of the other Or-ing diodes, D3, D4 or D5. When the Or-ing diodes are installed the parallel jumper would not be populated. The diode drop will be subtracted from the output voltage regulation point, so it is recommended to change the feedback resistors or select a higher output voltage setpoint to compensate for the diode drop.

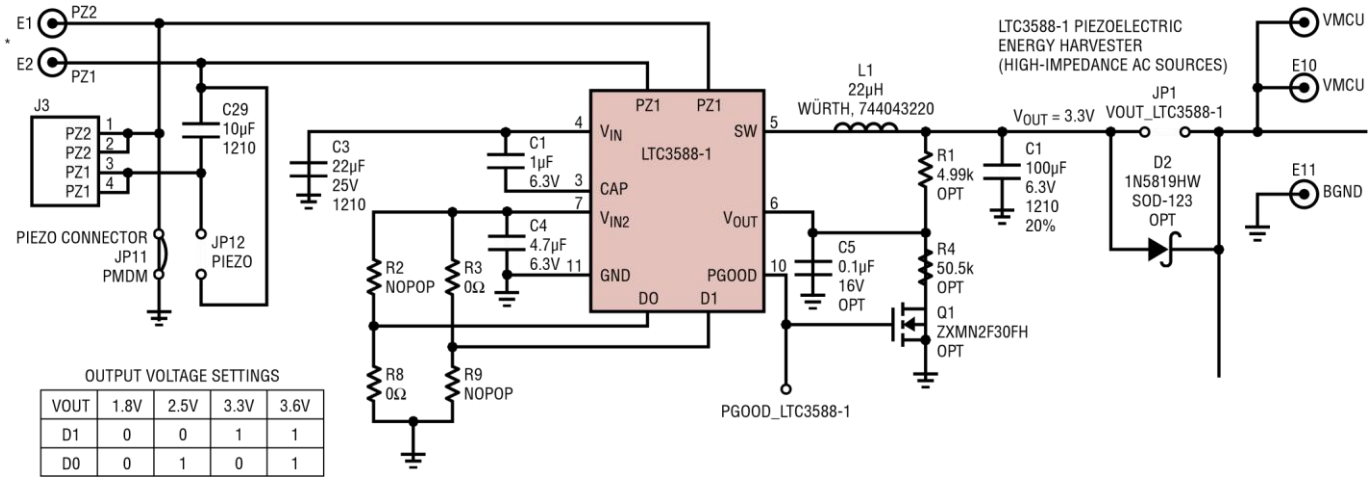

OUTPUT VOLTAGE SETTINGS

VOUT	1.8V	2.5V	3.3V	3.6V
D1	0	0	1	1
D0	0	1	0	1

When more than one of these diodes is installed and the associated energy harvester inputs are powered, the

DC2080A F06

V_{IN}*	I_{IN}
≤ $18V_{PK}$	≤50mA
> $18V_{PK}$	≤5mA

Figure 6. Detailed Schematic of LTC3588-1 Piezoelectric Energy Harvesting Power Supply

APPLICATION

board will switch between energy harvester power circuits as needed to maintain the output voltage.

LTC3108: TEG Powered Energy Harvester The LTC3108 TEG powered energy harvester is selected by installing the power selection jumper JP2. The PGOOD signal, PGOOD_LTC3108 can be routed to the header by installing Jumper JP6. The LTC3108 PGOOD signal is pulled up to the on-chip 2.2V LDO through a 1MΩ pullup resistor.

If the application requires a wide hysteresis window for the PGOOD signal, please refer to the above section for a complete operational description of and how to use the independent PGOOD signal (PGOOD_LTC3459), shown in Figure 10, generated by the LTC2935-2 and available on JP8.

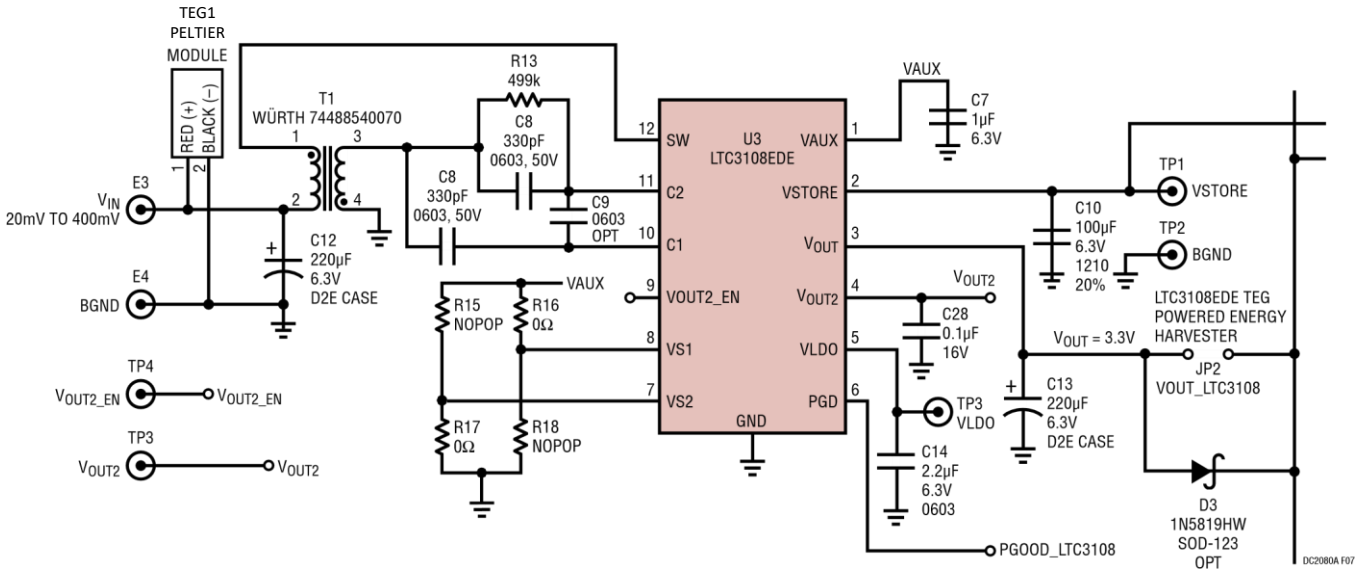

Figure 7. Detailed Schematic of LTC3108 TEG Powered Energy Harvester

The PGOOD_LTC3459 signal is always used to switch the output voltage on the header. Some loads do not like to see a slowly rising input voltage. Switch Q3 ensures that VMCU on the header is off until the energy harvested output voltage is high enough to power the load.

When the PGOOD signal from the LTC3108 is used as the header signal, the setpoint for the LTC2935-2 circuit needs to be changed so the turn-on threshold is below the PGOOD_LTC3108 turn-on threshold of 3.053V. For example, by changing R36 to a 0Ω Jumper and R5 to NOPOP, the turn-on threshold for Q3 will be 2.99V rising and 2.25V falling.

Diode D3 is an optional component used to diode-OR multiple energy harvesting sources together. This diode would be used in conjunction with one or more of the other Or-ing diodes, D2, D4 or D5. When the Or-ing diodes are installed the parallel jumper would not be populated. The diode drop will be subtracted from the output voltage setpoint, so it is recommended to change the feedback resistors or select a higher output voltage

APPLICATION

setpoint to compensate for the diode drop. When more than one of these diodes is installed and the associated energy harvester inputs are powered, the board will switch between energy harvester power circuits as needed to maintain the output voltage.

LTC3105: Supplied By Diode Voltage Drop In 4mA to 20mA Loop

The LTC3105 4-20mA Loop, Diode Voltage Drop powered energy harvester is selected by installing the power selection jumper JP3. The PGOOD signal, PGOOD_LTC3105 can be routed to the Header by installing Jumper JP7. The PGOOD_LTC3105 signal is an open-drain output. The pull-down is disabled at the beginning of the first sleep event after the output voltage has risen above 90% of its regulation value.

PGOOD_LTC3105 remains asserted until V_{OUT} drops below 90% of its regulation value at which point PGOOD_LTC3105 will pull low. The pull-down is also disabled while the IC is in shutdown or start-up mode.

If the application would benefit from a wider PGOOD hyteresis window than the LTC3105 provides (sleep to V_{OUT} minus 10%), the PGOOD_LTC3459 signal can be used in place of any of the PGOOD signals generated by the harvester circuits.

The PGOOD_LTC3459 signal is always used to switch the output voltage on the header. Some loads do not like to see a slowly rising input voltage. Switch Q3 ensures that VMCU on the header is off until the energy harvested output voltage is high enough to power the load.

The optional components shown on the schematic are not populated for a standard assembly. The function of R22 and Q2 is to generate a short PGOOD pulse that will indicate when the output capacitor is charged to its maximum value. The short pulse occurs every time the output capacitor charges up to the output sleep threshold, which for a 3.3V output is 3.312V. By populating these components the application can use this short pulse as a sequence timer to step through the program sequence or as an indication of when it can perform energy intensive functions, such as a sensor read or a wireless transmission and/or receive, knowing precisely how much charge is available in the output

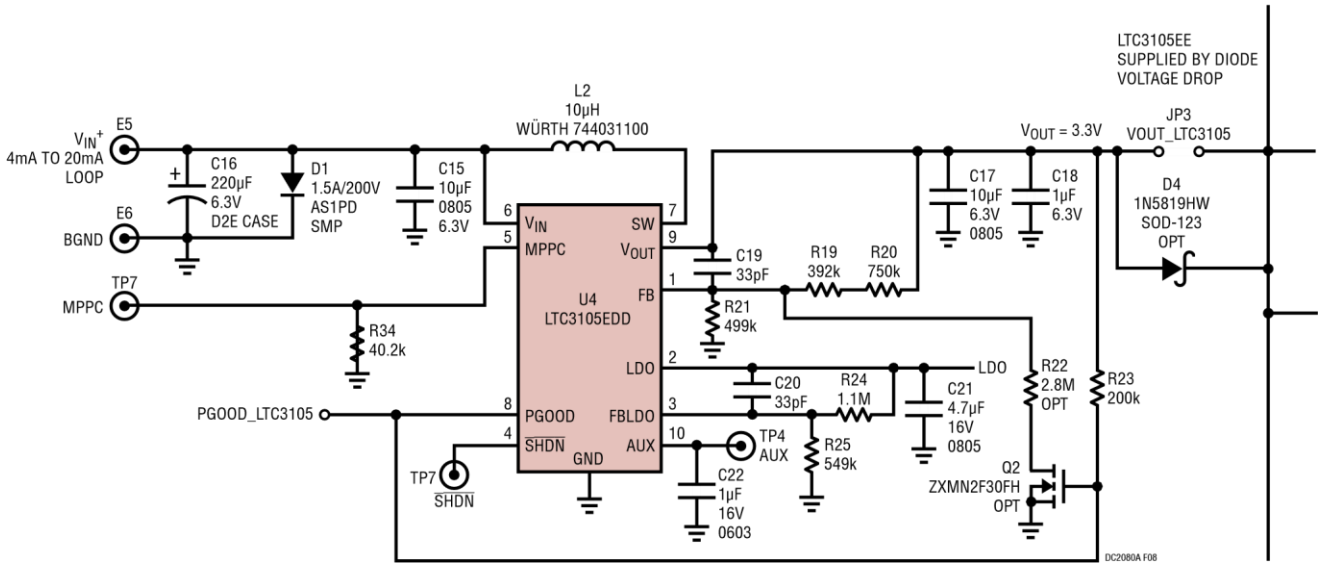

Figure 8. Detailed Schematic of LTC3105 4mA to 20mA Loop, Diode Voltage Drop Energy Harvester

APPLICATION

capacitors. When this optional circuit is not used, the amount of charge in the output capacitors is anywhere between the maximum (COUT • VOUT_SLEEP) to ten percent low. In the case where the energy harvesting source can support the average load continuously, this optional circuit is not needed.

Diode D4 is an optional component used to Diode-OR multiple energy harvesting sources together. This diode would be used in conjunction with one or more of the other Or-ing diodes, D2, D3 or D5. When the Or-ing diodes are installed the parallel jumper would not be populated. The diode drop will be subtracted from the output voltage setpoint so it is recommended to change the feedback resistors

D6 (SOLAR PANEL)
AM-5412

or select a higher output voltage setpoint to compensate for the diode drop. When more than one of these diodes is installed and the associated energy harvester inputs are powered, the board will switch between energy harvester power circuits as needed to maintain the output voltage.

LTC3459 Supplied By Solar Cell

The LTC3459 solar powered energy harvester is selected by installing the power selection jumper JP4. The PGOOD signal, PGOOD_LTC3459 can be routed to the Header by installing Jumper JP8.

The LTC2935-4 adds a hysteretic input-voltage regulation function to the LTC3459 application circuit. The PFO output of the LTC2935-4 is connected to the SHDN input on the LTC3459, which means that the LTC3459 will be off until VIN_LTC3459 rises above 1.743V (1.72V + 2.5%) and will then turn off when VIN_LTC3459 falls below 1.72V. The result is that the input voltage to the LTC3459 circuit will be regulated to, 1.73V, the average of the LTC2934-4 rising and falling PFO thresholds. The threshold can be adjusted for the peak operating point of the solar panel selected. In this design, because the LTC3459 output is set to 3.3V and is a boost topology, the input voltage is limited to 3.3V.

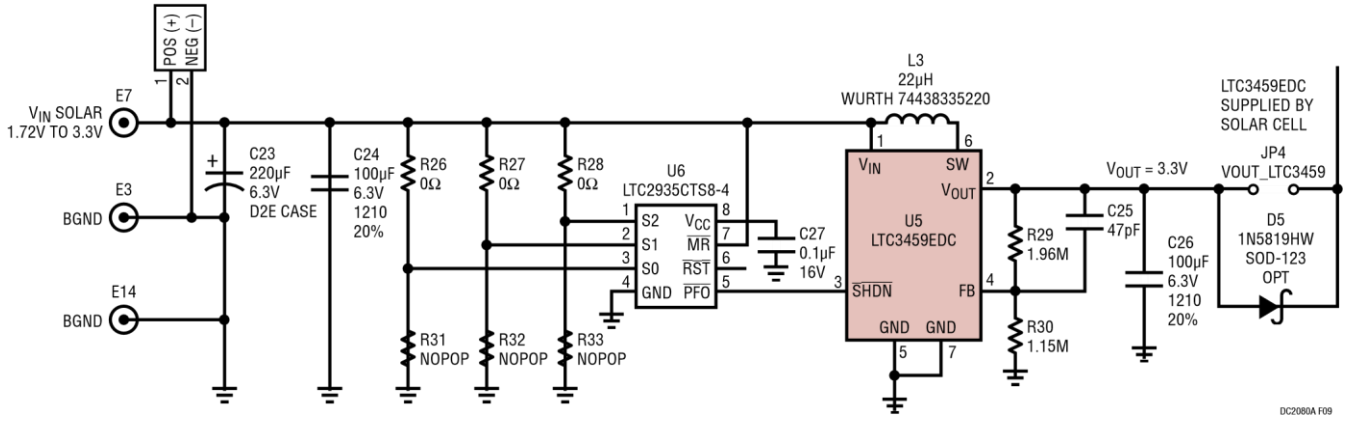

Figure 9. Detailed Schematic of LTC3459 Supplied by a Solar Cell

APPLICATION

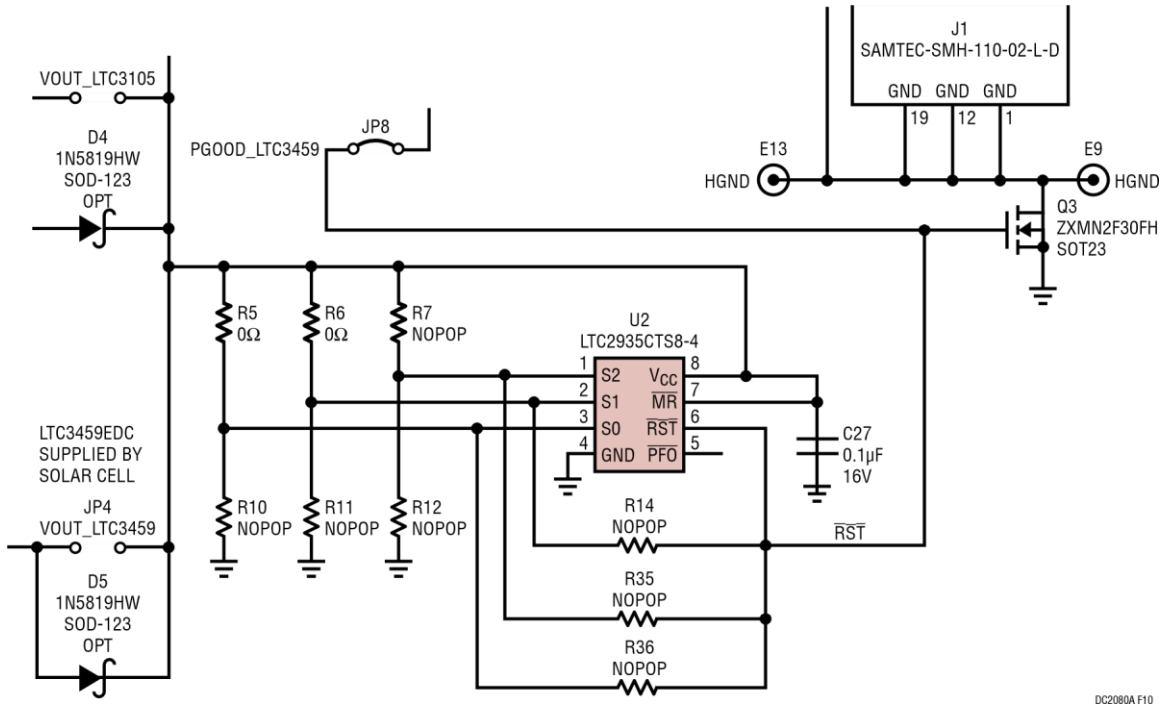

Figure 10. Detailed Schematic of PGOOD_LTC3459 Circuit Using LTC2935-2

The LTC3459 does not have an internally generated PGOOD signal so the LTC2935-2 was used to generate a PGOOD function with an adjustable hysteresis window. The NOPOP and 0Ω resistors around the LTC2935-2 allow for customization of the PGOOD thresholds and hysteresis window. By using R14, R35 and R36 the inputs can be changed after the rising Threshold is reached, creating a large hysteresis window.

The PGOOD_LTC3459 signal can be used in place of any of the PGOOD signals generated by the harvester circuits. The PGOOD_LTC3459 signal is always used to switch the output voltage on the header. The board is configured from the factory to use the PGOOD_LTC3459 signal as the PGOOD signal to switch from battery power to energy harvesting power.

The PGOOD_LTC3459 signal is always used to switch the output voltage on the header. Some loads do not like to see a slowly rising input voltage. Switch Q3 ensures that VMCU on the header is off until the energy harvested output voltage is high enough to power the load. The LTC2935-2 is configured to turn on Q3 at 3.15V and turn off Q3 at 2.25V. With this circuit, the load will see a fast voltage rise at start-up and be able to utilize all the energy stored in the output capacitors between the 3.15V and 2.25V levels. Diode D5 is an optional component used to Diode-OR multiple energy harvesting sources together. This diode would be used in conjunction with one or more of the other Or-ing diodes, D2, D3 or D4. When the Or-ing diodes are installed the parallel jumper would not be populated.

APPLICATION

The diode drop will be subtracted from the output voltage setpoint, so it is recommended to change the feedback resistors or select a higher output voltage setpoint to compensate for the diode drop. When more than one of these diodes is installed and the associated energy harvester inputs are powered, the board will switch between energy harvester power circuits as needed to maintain the output voltage.

PARTS LIST

ITEM	QTY	REFERENCE	PART DESCRIPTION	MANUFACTURER/PART NUMBER
Required Circuit Components				
1	3	C1, C7, C18	CAP, CHIP, X5R, 1µF, 10%, 6.3V, 0402	TDK, C1005X5R0J105KT
2	4	C2, C10, C24, C26	CAP, CHIP, X5R, 100µF, 20%, 10V, 1210	TAIYO YUDEN, LMK325ABJ107MM
	15	C01 - C015 (OPTIONAL ENERGY STORAGE)		
3	1	C3	CAP, CHIP, X5R, 22µF, 10%, 25V, 1210	AVX, 12103D226KAT2A
4	1	C4	CAP, CHIP, X5R, 4.7µF, 10%, 6.3V, 0603, Height = 0.80mm	TDK, C1608X5R0J475K/0.80
5	3	C6, C27, C28	CAP, CHIP, X7R, 0.1µF, 10%, 16V, 0402	MURATA, GRM155R71C104KA88D
6	1	C8	CAP, CHIP, X7R, 330pF, 50V, 10%, 0603	MURATA, GRM188R71H331KA01D
7	1	C11	CAP, CHIP, X7R, 1000pF, 50V, 10%, 0603	MURATA, GRM188R71H102KA01D
8	4	C12, C13, C16, C23	CAP, POLYMER SMD, 220µF, 6.3V, 18mΩ, 2.8Arms, D2E CASE	SANYO, 6TPE220MI
9	1	C14	CAP, CHIP, X5R, 2.2µF, 16V, 10%, 0603	MURATA, GRM188R61C225KE15D
10	2	C15, C17	CAP, CHIP, X5R, 10µF, 10%, 6.3V, 0805	AVX, 08056D106KAT2A
11	2	C19, C20	CAP, CHIP, NPO, 33pF, 5%, 25V, 0402	AVX, 04023A330JAT2A
12	1	C21	CAP, CHIP, X5R, 4.7µF, 10%, 16V, 0805	TAIYO YUDEN, EMK212BJ475MG-T
13	1	C22	CAP, CHIP, X5R, 1µF, 10%, 16V, 0603	AVX, 0603YD105KAT2A
14	1	C25	CAP, CHIP, NPO, 47pF, 5%, 25V, 0402	AVX, 04023A470JAT2A
15	1	C29	CAP, CHIP X5R, 10µF,10%, 25V,1210	AVX, 12103D106KAT2A
16	1	D1	DIODE, STANDARD, 200V, 1.5A, SMP	VISHAY, AS1PD-M3/84A
17	1	D6	SANYO, AMORPHOUS SOLAR CELL	SANYO, AM-5412
18	1	HS1	HEAT SINK, 50.8mm × 50mm	FISCHER, SK 426
19	1	L1	INDUCTOR, 22µH , 0.70A, 185mΩ, 4.8mm × 4.8mm	WÜRTH, 744043220
20	1	L2	INDUCTOR, 10µH, 560mA, 0.205Ω, 3.8mm × 3.8mm	WÜRTH, 744031100
21	1	L3	INDUCTOR, 22µH, 600mA, 940mΩ, 3mm × 3mm	WÜRTH, 74438335220
22	1	T1	TRANSFORMER, 100:1 TURNS RATIO	WÜRTH, 74488540070
23	1	TEG1	PELTIER MODULE CP85438	CUI INC., CP85438
24	1	Q3	N-CHANNEL MOSFET, 20V, SOT23	DIODES/ZETEX, ZXMN2F30FHTA
25	11	R1, R3, R5, R6, R8, R16, R17, R26, R27, R28, R35	RES, CHIP, 0Ω JUMPER, 1/16W, 0402	VISHAY, CRCW04020000Z0ED
26	2	R13, R21	RES, CHIP, 499kΩ, ±1%, 1/16W, 0402, ±100ppm/°C	VISHAY, CRCW0402499KFKED
27	1	R19	RES, CHIP, 392kΩ, ±1%, 1/16W, 0402, ±100ppm/°C	VISHAY, CRCW0402392KFKED
28	1	R20	RES, CHIP, 750kΩ, ±1%, 1/16W, 0402, ±100ppm/°C	VISHAY, CRCW0402750KFKED
29	1	R23	RES, CHIP, 200kΩ, ±1%, 1/16W, 0402, ±100ppm/°C	VISHAY, CRCW0402200KFKED
30	1	R24	RES, CHIP, 1.10MΩ, ±1%, 1/16W, 0402, ±100ppm/°C	VISHAY, CRCW04021M10FKED
31	1	R25	RES, CHIP, 549kΩ, ±1%, 1/16W, 0402, ±100ppm/°C	VISHAY, CRCW0402549KFKED

32	1	R29	RES, CHIP, 1.96MΩ, ±1%, 1/16W, 0402, ±100ppm/°C	VISHAY, CRCW04021M96FKED
33	1	R30	RES, CHIP, 1.15MΩ, ±1%, 1/16W, 0402, ±100ppm/°C	VISHAY, CRCW04021M15FKED
34	1	R34	RES, CHIP, 40.2kΩ, ±1%, 1/16W, 0402, ±100ppm/°C	VISHAY, CRCW040240K2FKED
35	1	U1	PIEZOELECTRIC ENERGY HARVESTING POWER SUPPLY, DFN 3mm × 3mm	ANALOG DEVICES, LTC3588EMSE-1
36	1	U2	IC, ULTRALOW POWER SUPERVISOR WITH POWER-FAIL OUTPUT, TSOT-23, 8-PIN	ANALOG DEVICES, LTC2935CTS8-2

PARTS LIST

ITEM	QTY	REFERENCE	PART DESCRIPTION	MANUFACTURER/PART NUMBER
37	1	U3	IC, ULTRALOW VOLTAGE STEP-UP CONVERTER AND POWER MANAGER, DFN 3mm × 4mm	ANALOG DEVICES, LTC3108EDE
38	1	U4	IC, 400mA STEP-UP DC/DC CONVERTER WITH MPPC AND 250mV START-UP, DFN 3mm × 3mm	ANALOG DEVICES, LTC3105EDD
39	1	U5	IC, 10V MICROPOWER SYNC BOOST CONVERTER, DFN 2mm × 2mm	ANALOG DEVICES, LTC3459EDC
40	1	U6	IC, ULTRALOW POWER SUPERVISOR WITH POWER-FAIL OUTPUT, TSOT-23, 8-PIN	ANALOG DEVICES, LTC2935CTS8-4
Additional Demo Board Circuit Components				
1	0	C5 (OPT)	CAP, CHIP, X7R, 0.1µF, 10%, 16V, 0402	MURATA, GRM155R71C104KA88D
2	0	C9 (OPT)	OPT, 0603	
3	0	D2 - D5 (OPT)	DIODE, SCHOTTKY, 40V, 1A, SOD-123	DIODES INC, 1N5819HW-7-F
4	0	Q1, Q2 (OPT)	N-CHANNEL MOSFET, 20V, SOT23	DIODES/ZETEX, ZXMN2F30FHTA
5	0	R1 (OPT)	RES, CHIP, 4.99KΩ, ±1%, 1/16W, 0402, ±100ppm/°C	VISHAY, CRCW04024K99FKED
6	0	R2, R7, R9, R10, R11, R12, R14, R15, R18, R31, R32, R33, R36	RES., CHIP, 0402	NOPOP
7	0	R4 (OPT)	RES, CHIP, 50.5kΩ, ±1%, 1/16W, 0402, ±100ppm/°C	VISHAY, CRCW040250K5FKED
8	0	R22 (OPT)	RES, CHIP, 2.80MΩ, ±1%, 1/16W, 0402, ±100ppm/°C	VISHAY, CRCW04022M80FKED
Hardware for Demo Board Only				
1	14	E1 - E14	TURRET, 0.061 DIA	MILL-MAX, 2308-2
2	10	JP1 - JP8, JP11, JP12	HEADER, 2 PINS, 2mm	SAMTEC, TMM-102-02-L-S
3	2	JP9, JP10	HEADER, 3 PINS, 2mm	SAMTEC, TMM-103-02-L-S
4	3	JP4, JP9, JP11	SHUNT 2mm	SAMTEC, 2SN-BK-G
5	0	JP1, JP2, JP3, JP5, JP6, JP7, JP8, JP10, JP12	SHUNT 2mm, (DO NOT INSTALL)	SAMTEC, 2SN-BK-G
6	1	J1	HEADER, 2×10, 20-PIN, SMT HORIZONTAL SOCKET, 0.100"	SAMTEC, SMH-110-02-L-D
7	0	J2 (OPT)	HEADER, 2×6, 12-PIN, SMT HORIZONTAL SOCKET WITH KEY, 0.100"	SAMTEC, SMH-106-02-L-D-05
8	1	J3	PIEZO CONNECTOR 4 PIN, TERMINAL BLOCK, WR-TBL	WÜRTH, 691411710002

9	4		ADHESIVE CABLE MOUNT U-STYLE CLIP	WÜRTH, 523252000
10	1		KERAFOL, KL 90 40mm × 40mm × 3mm DOUBLE-SIDED ADHESIVE TAPE	KERATHERM, KL 90 40mm × 40mm × 3mm
11	0.007		DOUBLE-SIDED MOUNTING TAPE, 35mm × 38mm FOR SOLAR CELL	TESA, 55742 (KIT QTY = NUMBER OF REELS, ROUND UP)

SCHEMATIC DIAGRAM

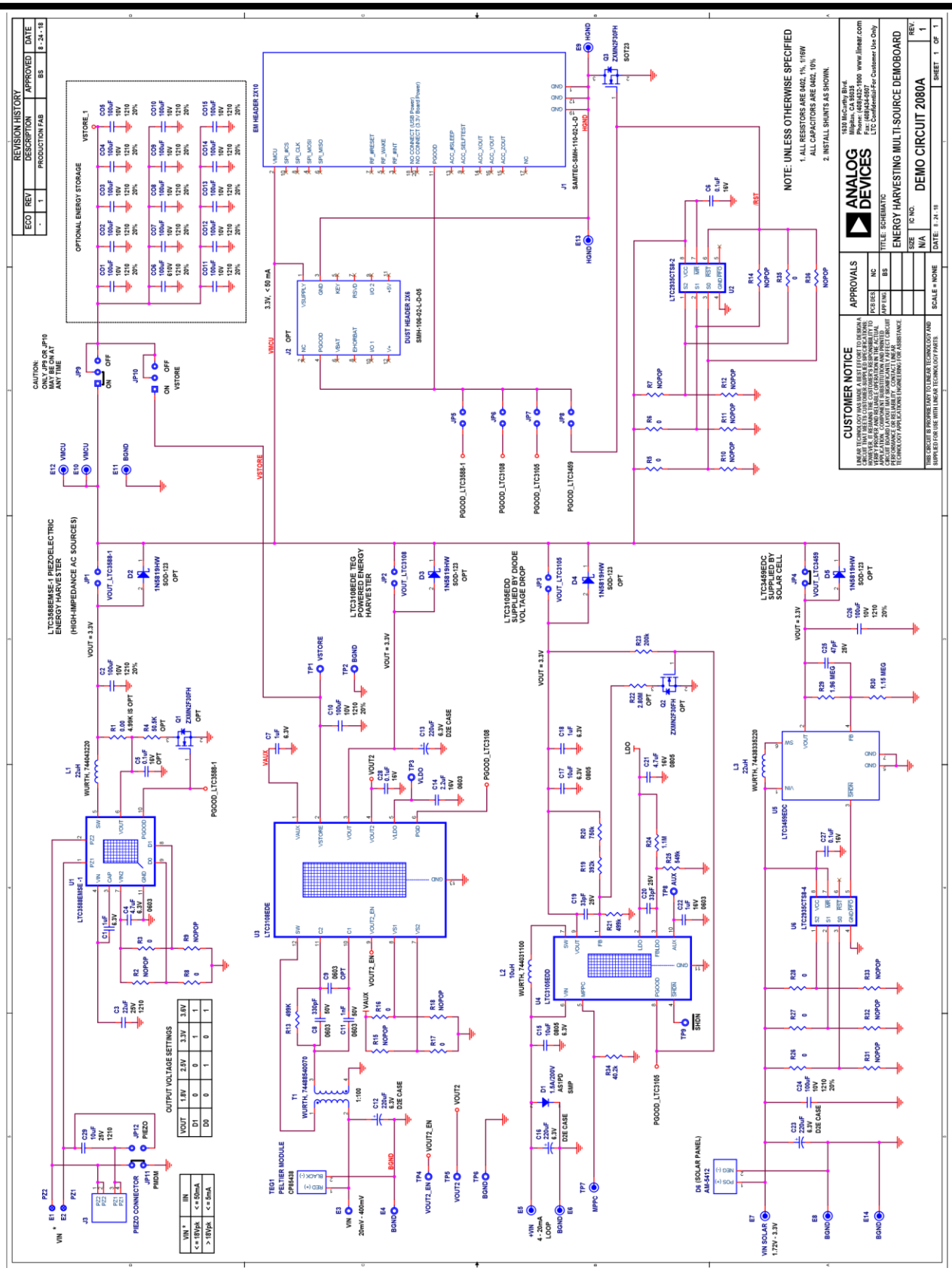
REVISION HISTORY
ECO REV DESCRIPTION APPROVED DATE
- 1 PRODUCTION FAB BS 8-24-18
OPTIONAL ENERGY STORAGE
VSTORE_1
EIM HEADER 2X10
DUST HEADER 2X6
SMH-106-02-L-D-05
SAMTEC-SMH-110-02-L-D
LTC3588SENSE-1 PIEZOELECTRIC ENERGY HARVESTER (HIGH-IMPEDANCE AC SOURCES)
LTC3108EDE TEG POWERED ENERGY HARVESTER
LTC3105EDD SUPPLIED BY DIODE VOLTAGE DROP
LTC3459EDC SUPPLIED BY SOLAR CELL
TEG1 PELTIER MODULE CP85438
D6 (SOLAR PANEL) AM-5412
OUTPUT VOLTAGE SETTINGS
VOUT 1.8V 2.2V 3.3V 3.6V
D1 0 0 1 1
D0 0 1 0 1
VIN* IIN
<= 18Vpk <= 60mA
> 18Vpk <= 5mA
CAUTION: ONLY JP9 OR JP10 MAY BE ON AT ANY TIME
NOTE: UNLESS OTHERWISE SPECIFIED
1. ALL RESISTORS ARE 0402, 1%, 1/16W
ALL CAPACITORS ARE 0402, 10%
2. INSTALL SHUNTS AS SHOWN.
CUSTOMER NOTICE
ANALOG DEVICES
1630 McCarthy Blvd.
Milpitas, CA 95035
Phone: (408)432-1900 www.linear.com
Fax: (408)434-0507
LTC Confidential-For Customer Use Only
TITLE: SCHEMATIC
ENERGY HARVESTING MULTI-SOURCE DEMOBOARD
SIZE IC NO. DEMO CIRCUIT 2080A REV. 1
N/A
DATE: 8, 24, 18 SHEET 1 OF 1
APPROVALS
PCB DES. NC
APP ENG. BS
SCALE = NONE
THIS CIRCUIT IS PROPRIETARY TO LINEAR TECHNOLOGY AND SUPPLIED FOR USE WITH LINEAR TECHNOLOGY PARTS.

ESD Caution

ESD (electrostatic discharge) sensitive device. Charged devices and circuit boards can discharge without detection. Although this product features patented or proprietary protection circuitry, damage may occur on devices subjected to high energy ESD. Therefore, proper ESD precautions should be taken to avoid performance degradation or loss of functionality.

Legal Terms and Conditions

By using the evaluation board discussed herein (together with any tools, components documentation or support materials, the "Evaluation Board"), you are agreeing to be bound by the terms and conditions set forth below ("Agreement") unless you have purchased the Evaluation Board, in which case the Analog Devices Standard Terms and Conditions of Sale shall govern. Do not use the Evaluation Board until you have read and agreed to the Agreement. Your use of the Evaluation Board shall signify your acceptance of the Agreement. This Agreement is made by and between you ("Customer") and Analog Devices, Inc. ("ADI"), with its principal place of business at One Technology Way, Norwood, MA 02062, USA. Subject to the terms and conditions of the Agreement, ADI hereby grants to Customer a free, limited, personal, temporary, non-exclusive, non-sublicensable, non-transferable license to use the Evaluation Board FOR EVALUATION PURPOSES ONLY. Customer understands and agrees that the Evaluation Board is provided for the sole and exclusive purpose referenced above, and agrees not to use the Evaluation Board for any other purpose. Furthermore, the license granted is expressly made subject to the following additional limitations: Customer shall not (i) rent, lease, display, sell, transfer, assign, sublicense, or distribute the Evaluation Board; and (ii) permit any Third Party to access the Evaluation Board. As used herein, the term "Third Party" includes any entity other than ADI, Customer, their employees, affiliates and in-house consultants. The Evaluation Board is NOT sold to Customer; all rights not expressly granted herein, including ownership of the Evaluation Board, are reserved by ADI. CONFIDENTIALITY. This Agreement and the Evaluation Board shall all be considered the confidential and proprietary information of ADI. Customer may not disclose or transfer any portion of the Evaluation Board to any other party for any reason. Upon discontinuation of use of the Evaluation Board or termination of this Agreement, Customer agrees to promptly return the Evaluation Board to ADI. ADDITIONAL RESTRICTIONS. Customer may not disassemble, decompile or reverse engineer chips on the Evaluation Board. Customer shall inform ADI of any occurred damages or any modifications or alterations it makes to the Evaluation Board, including but not limited to soldering or any other activity that affects the material content of the Evaluation Board. Modifications to the Evaluation Board must comply with applicable law, including but not limited to the RoHS Directive. TERMINATION. ADI may terminate this Agreement at any time upon giving written notice to Customer. Customer agrees to return to ADI the Evaluation Board at that time. LIMITATION OF LIABILITY. THE EVALUATION BOARD PROVIDED HEREUNDER IS PROVIDED "AS IS" AND ADI MAKES NO WARRANTIES OR REPRESENTATIONS OF ANY KIND WITH RESPECT TO IT. ADI SPECIFICALLY DISCLAIMS ANY REPRESENTATIONS, ENDORSEMENTS, GUARANTEES, OR WARRANTIES, EXPRESS OR IMPLIED, RELATED TO THE EVALUATION BOARD INCLUDING, BUT NOT LIMITED TO, THE IMPLIED WARRANTY OF MERCHANTABILITY, TITLE, FITNESS FOR A PARTICULAR PURPOSE OR NONINFRINGEMENT OF INTELLECTUAL PROPERTY RIGHTS. IN NO EVENT WILL ADI AND ITS LICENSORS BE LIABLE FOR ANY INCIDENTAL, SPECIAL, INDIRECT, OR CONSEQUENTIAL DAMAGES RESULTING FROM CUSTOMER'S POSSESSION OR USE OF THE EVALUATION BOARD, INCLUDING BUT NOT LIMITED TO LOST PROFITS, DELAY COSTS, LABOR COSTS OR LOSS OF GOODWILL. ADI'S TOTAL LIABILITY FROM ANY AND ALL CAUSES SHALL BE LIMITED TO THE AMOUNT OF ONE HUNDRED US DOLLARS ($100.00). EXPORT. Customer agrees that it will not directly or indirectly export the Evaluation Board to another country, and that it will comply with all applicable United States federal laws and regulations relating to exports. GOVERNING LAW. This Agreement shall be governed by and construed in accordance with the substantive laws of the Commonwealth of Massachusetts (excluding conflict of law rules). Any legal action regarding this Agreement will be heard in the state or federal courts having jurisdiction in Suffolk County, Massachusetts, and Customer hereby submits to the personal jurisdiction and venue of such courts. The United Nations Convention on Contracts for the International Sale of Goods shall not apply to this Agreement and is expressly disclaimed.

Rev.A

09/18 www.analog.com